PHOTOSAT

CASE STUDY

Rapid. Accurate. Reliable.

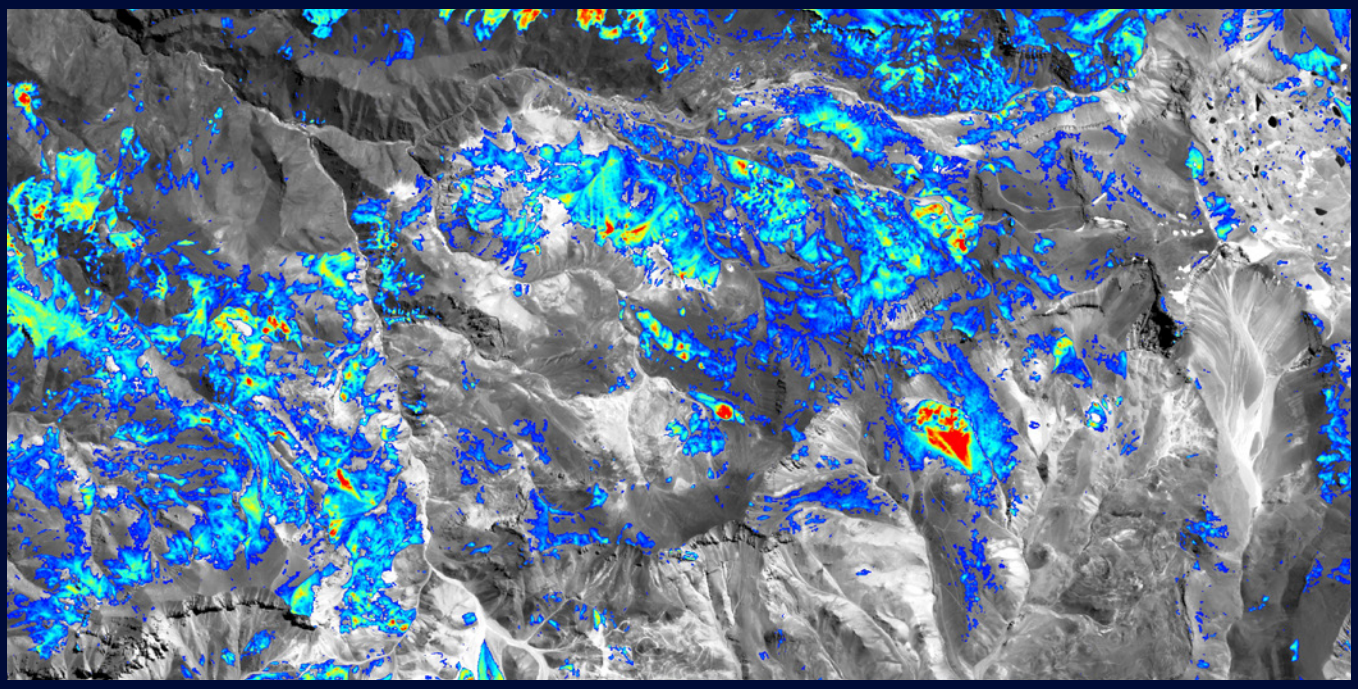

# Cerro Casale & Caspiche
## Regional Hyperspectral Exploration Targeting (R-HET)

THE NEXT GENERATION OF SATELLITE ALTERATION MINERAL MAPPING

Photosat Information LTD. | 580-1188 West Georgia Street, Vancouver BC V6A4E2

# Contents



# Abstract


The Cerro Casale and Caspiche gold-copper deposits are situated in the Maricunga Belt of northern Chile, approximately 110 km southeast of Copiapó.

The Maricunga Belt encompasses numerous large hydrothermal alteration zones hosted by volcanic rocks and high-level stocks that intruded them. Mineralization includes gold +/- copper-rich porphyry and precious-metal epithermal styles, formed during late Oligocene and Miocene hydrothermal events (Sillitoe et al. 1991). Both deposits were discovered in the 1980s and have undergone extensive exploration. Currently, the two deposits form the Norte Abierto project, which is part of the Norte Abierto JV between Newmont and Barrick.

In this report, PhotoSat showcases the results from the new Regional Hyperspectral Exploration Targeting (R-HET) product over the Cerro Casale and Caspiche region. For results, read the full case study report.


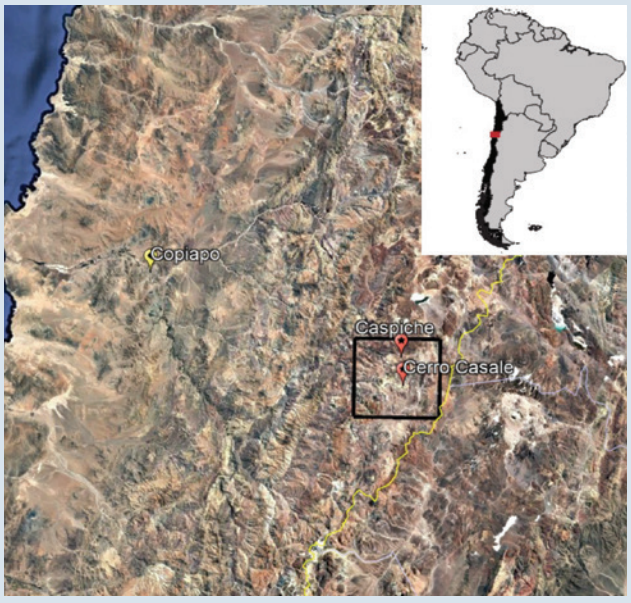


**Figure 1.** Location of the Cerro Casale and Caspiche deposits in northern Chile. The region analyzed in this case study is shown by the black rectangle.

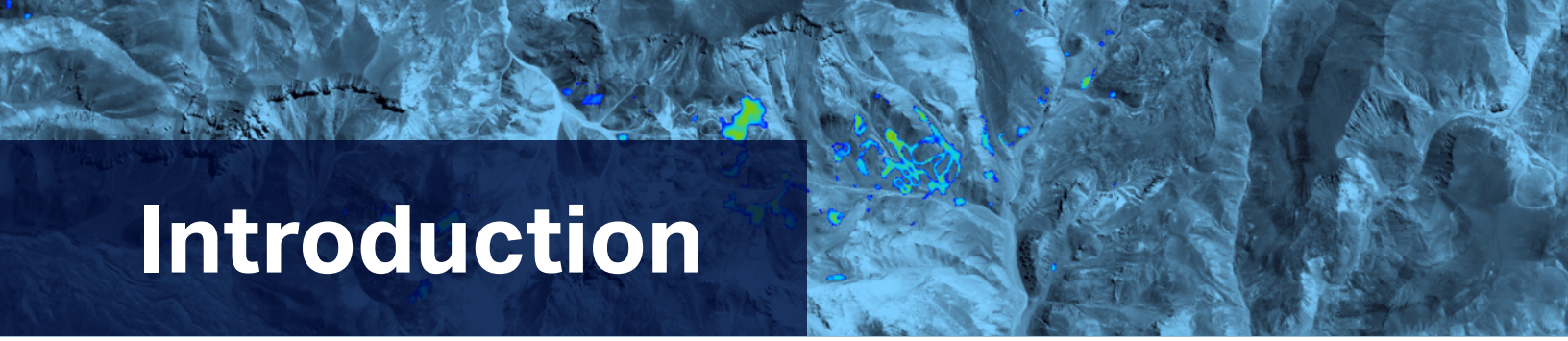

# Introduction

**This case study details the results of PhotoSat's Regional Hyperspectral Exploration Targeting (R-HET) solution over the Cerro Casale and Caspiche deposit region in the southern part of the Maricunga Volcanic Belt.**

## Regional Geology

The Cerro Casale and Caspiche gold-copper deposits form the Norte Abierto project, which is part of the Norte Abierto JV between Newmont and Barrick. The project currently has a proven and probable reserve of 23.2 million ounces of gold and 5.8 billion pounds of copper.

The Cerro Casale and Caspiche deposits are in the Aldebaran sub-district of the Maricunga Volcanic Belt. The Maricunga Belt comprises a series of coalescing composite, Miocene andesitic to rhyolitic volcanic centres that extend for 200 km along the western crest of the Andes.

Reverse faults parallel to the axis of the Andes have caused uplift of hypabyssal intrusive rocks beneath the extrusive volcanics. In turn, this uplift has exposed porphyry-hosted gold and copper deposits in the Aldebaran region. (Palacios, et al, 2001)

## Cerro Casale Deposit

At Cerro Casale, gold-copper mineralization occurs in quartz-sulfide and quartz-magnetite-specularite veinlet stockworks developed in dioritic to granodioritic intrusives and in adjacent intermediate to felsic volcanic rocks. Mineralization appears to be most closely related to strong potassic to phyllic alteration of the latest phases of intermediate to felsic intrusives and associated intrusive and hydrothermal breccias. Cerro Catedral is believed to represent the original lithocap of the alteration system, characterized by abundant alunite, kaolinite, and chalcedonic silica (Henderson, R., & Eng, P., 2010).

## Caspiche Deposit

The Caspiche deposit lies 12 km north of the Cerro Casale deposit. At Caspiche, gold-copper mineralization is centred on a composite diorite to quartz diorite porphyry stock intruding felsic volcanic rocks. Within the deposit, five outward-younging phases are routinely distinguished.

The gold-copper mineralization in the lower half of the deposit is accompanied by quartz ± magnetite-veined, potassic-altered rocks. Shallower mineralization occurs within quartz-kaolinite-dominated, advanced argillic alteration. The upper parts of the advanced argillic zone are characterized by siliceous ledges, some of which are auriferous, composed of vuggy residual quartz and/or silicified rock.

A relatively minor, shallowly inclined zone of intermediate sulfidation epithermal gold-zinc mineralization, comprising narrow veinlets and disseminations, abuts a late-mineral diatreme

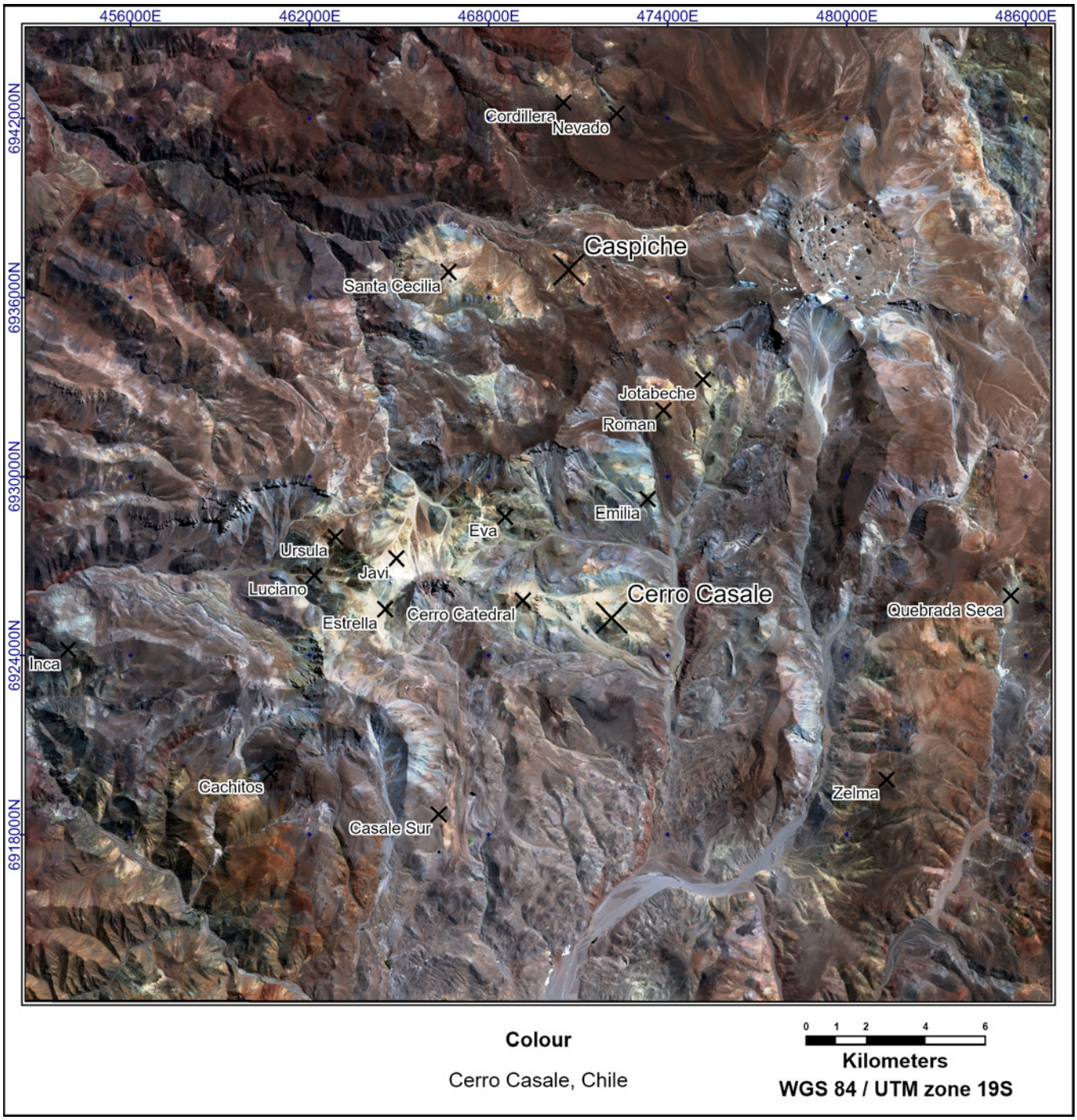


**Figure 2.** Case study area. Natural colour image showing a regional overview of the project area. Cerro Casale & Caspiche locations are shown with a large black X, satellite deposit locations (Roman, Jotabeche, Eva, Emilia, etc.) are shown with a small black x.

contact. Post-mineral volcanics cover much of the area in the north of the property. Quaternary colluvium overlies most of the property (Sillitoe et al, 2013).

## Other Deposits in the Region

Cerro Casale and Caspiche have been the focus of the Aldebaran region due to their immense size; many other nearby showings/deposits have been explored. This includes Eva, Roman, Jotabeche, and Javi, which exhibit similar mineralization styles to Cerro Casale and Caspiche and have the potential to host similar scales of resources (Henderson, R., & Eng, P., 2010).

This regional report also includes exploration projects owned by other companies, such as Cachitos, Casale Sur, Zelma (Gold Hart Resources), Santa Cecelia (Torq Resources), Inca (Stuve Gold Corp), Cordillera (Aero Energy), and Nevado (Teck).

# Methodology

## The Next Generation of Satellite Alteration Mineral Mapping

PhotoSat has developed proprietary deep-learning alteration mineral mapping processes, which utilize hyperspectral satellite data.

These solutions combine the benefits of various multi- and hyperspectral satellite sensors with PhotoSat's 20+ years of experience producing alteration mineral mapping products. These products are the "next generation" of satellite alteration mapping, which builds upon the capabilities of traditional multispectral solutions such as ASTER, Sentinel-2, and WorldView-3. The first product in this suite is a Regional Hyperspectral Exploration Targeting (R-HET) tool for high-quality regional exploration purposes.

R-HET combines the spectral resolution benefits of VNIR-SWIR hyperspectral sensors, such as EMIT, with the spatial benefits of Sentinel-2, and TIR data from ASTER to provide geologists with the information needed to make the best possible data-driven decisions when generating targets for area selection and project generation.

## Multispectral vs. Hyperspectral Satellites

Traditionally, the most widely used satellites for alteration mineral mapping utilize multispectral sensors (e.g., Landsat (1-9), Sentinel-2, ASTER, WorldView-3). Multispectral sensors typically collect 3 – 20 bands, with each band detecting a varying broad range of wavelengths across the electromagnetic (EM) spectrum.

### MULTISPECTRAL

Cannot confidently identify minerals when signatures are intensely mixed.

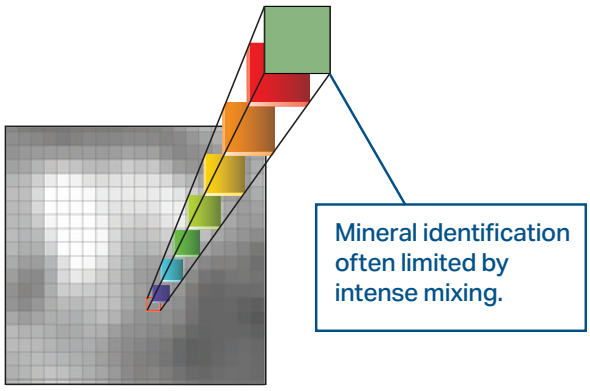


### HYPERSPECTRAL

High spectral resolution means minerals can be identified with higher confidence even when signatures are intensely mixed.

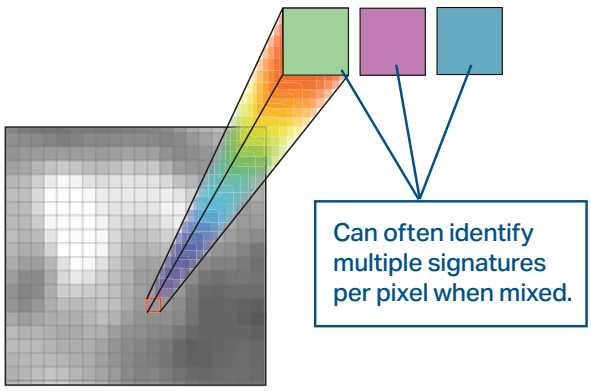


Cerro Casale & Caspiche Regional Hyperspectral Exploration Targeting (R-HET) - Case Study

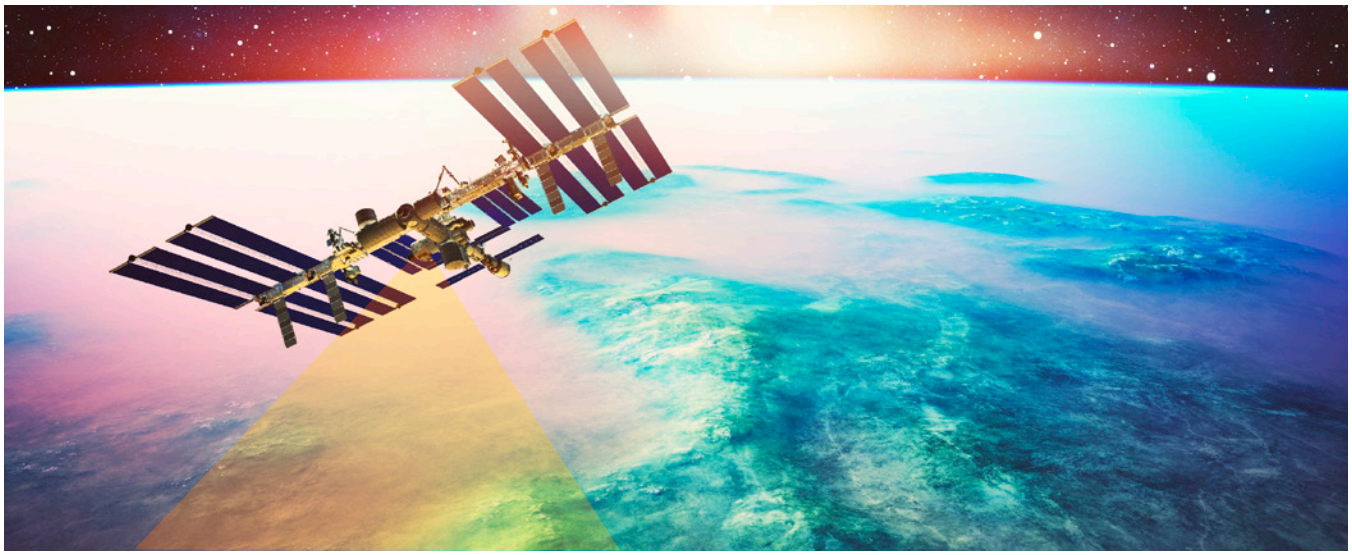

Hyperspectral sensors collect 100s of spectral bands where each band covers a much narrower wavelength range and has consistent band spacing. This type of spectral data is routinely collected by airborne, handheld, or core scanning hyperspectral sensors. Hyperspectral technology is now widely available through new spaceborne sensors, in particular ones that cover short-wave infrared (SWIR) wavelengths that are important for mineral identification, including EMIT, EnMAP, PRISMA, and Tanager.

Hyperspectral satellites typically have a coarser spatial resolution than their multispectral counterparts (for example, 60m for EMIT compared to 30m for ASTER). Still, the significantly enhanced spectral resolution substantially offsets this limitation. Regional HET (R-HET) leverages both the spatial benefits of multispectral sensors and the spectral benefits of hyperspectral sensors.

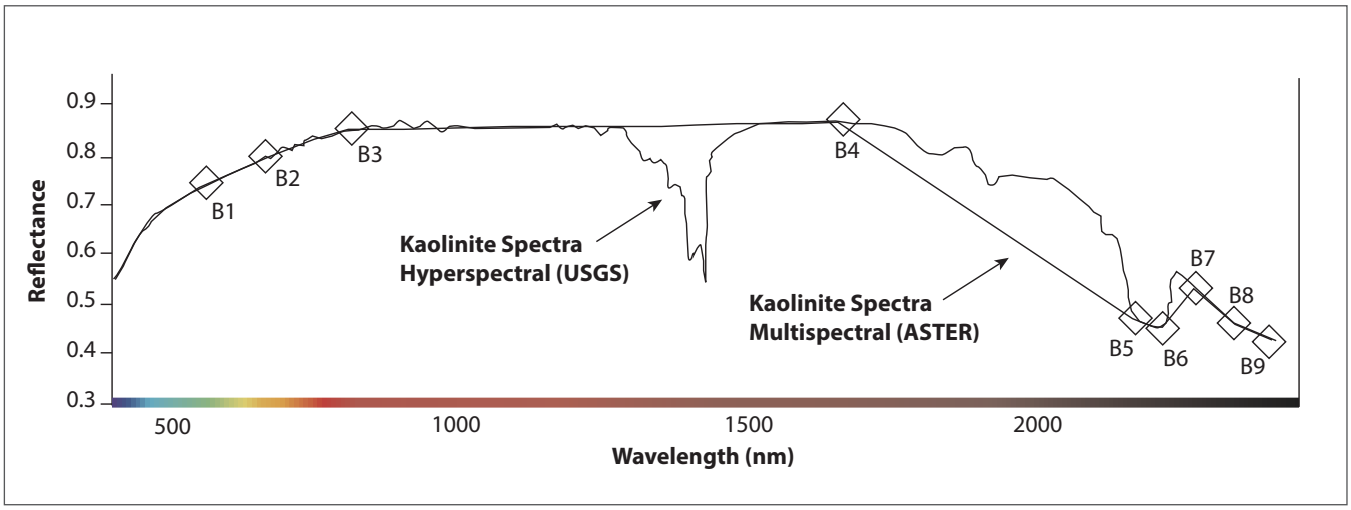


**Figure 3.** Comparison of ASTER multispectral response to USGS handheld hyperspectral response for kaolinite. The kaolinite hyperspectral response shows significantly more spectral detail not visible in the kaolinite ASTER response.

## EMIT Sensor

The hyperspectral data used in this case study was obtained from the EMIT (Earth Surface Mineral Dust Source Investigation) sensor, though the processing methods can be applied to other hyperspectral data and sensors. EMIT is a NASA mission originally intended to help researchers model global climate effects by measuring the surface mineral-dust sources using hyperspectral data over the world's deserts. The EMIT hyperspectral sensor was launched in 2022 and is installed on the International Space Station (ISS).

The EMIT sensor collects 285 contiguous narrow spectral bands across the Visible Near-Infrared (VNIR) and Short-Wave Infrared (SWIR) regions at a 48m x 60m ground resolution. There is an EMIT data archive starting from 2022, which primarily covers the world's arid regions and can extend up to 52° north and south latitudes.

Considering its spatial resolution, large swath sizes, and extensive archive data coverage, EMIT data is best suited for regional exploration purposes.

## Benefits of Hyperspectral Data

In addition to increasing the accuracy and reliability of mineral detection, using hyperspectral data enables the detection of a variety of new alteration minerals that were difficult to detect with available multispectral satellites, including minerals such as pyrophyllite, muscovite, and illite. It can also be used to differentiate crystallinities and compositions of minerals, such as high-Al muscovite vs low-Al muscovite and Fe-rich chlorite vs Mg-rich chlorite, as well as to estimate the relative abundances of some alteration minerals.

### Key benefits of using hyperspectral data include:

- Map/differentiate more key alteration minerals such as pyrophyllite, muscovite, and illite.
- Differentiate the compositions and crystallinities of minerals, such as K-alunite versus Na-alunite, or high-Al muscovite versus low-Al muscovite.
- Detect subtle subpixel alteration signatures in mixed spectra using advanced deep learning models, which improve accuracy and reduce false positives.
- Map the relative abundances of minerals to facilitate the development of more effective exploration targets.
- Compelling visuals help build a comprehensive model story for investors, executives, and other stakeholders.

**Figure 4.** Spectral and spatial characteristics of ASTER, Landsat-8, WV-3, and EMIT sensors.

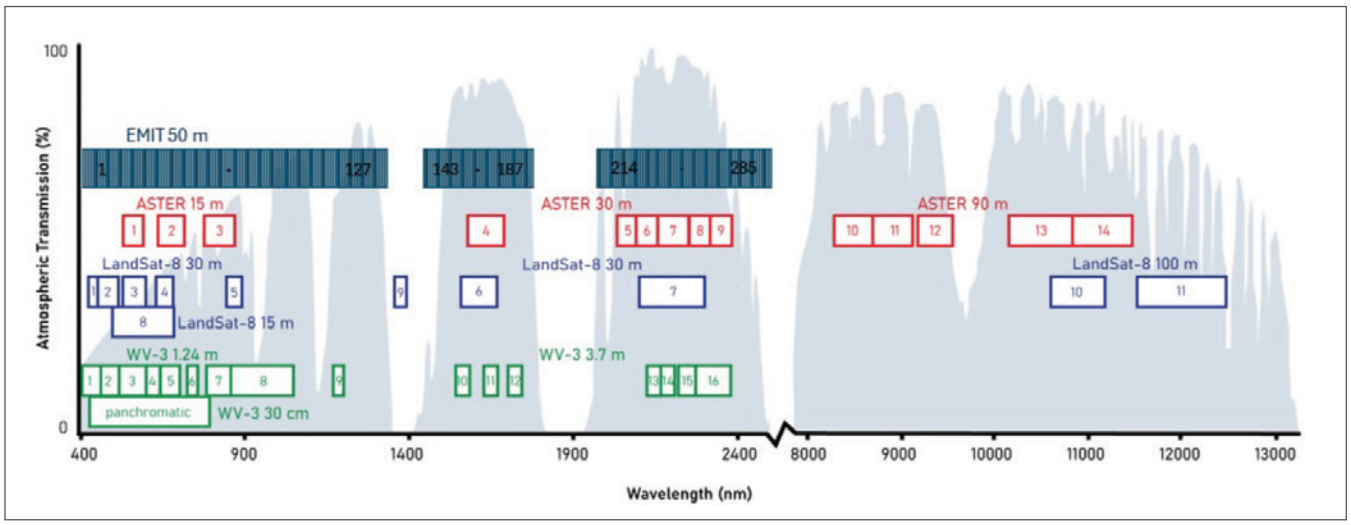

# Hyperspectral Mineral Identification

Launched in 2019, PhotoSat's proprietary deep-learning mineral mapping process utilizes spectral analysis algorithms to process satellite imagery. This process builds on PhotoSat's 20+ years of experience mapping alteration minerals using satellite data. Formerly applied to multispectral satellite datasets, this technology has been adapted to hyperspectral data processing.

Minerals have unique spectral characteristics that can be used to identify them. To positively identify a mineral, we look for and examine diagnostic features in the spectral profile or "signature".

### Spectral Feature Fitting

Minerals have unique absorption features in their spectral signature, which appear as local minima in the profile. The spectral profile of each pixel in a satellite image can be matched to diagnostic absorption features from reference spectral profiles of known minerals using resources such as the USGS Spectral Library. PhotoSat utilizes deep-learning algorithms to enhance this process, thereby improving the consistency and reliability of the results, particularly in highly complex spectra.

Additionally, PhotoSat maintains an internal library of reference spectral profiles, collected from various sources, for this purpose.

### Higher-Order Polynomial Fitting

Additional spectra attributes are extracted using a high-order polynomial fitting method. This method can analyze individual absorption features to extract criteria such as minimum depth, wavelength, asymmetry, and area. These attributes can be used to map mineral characteristics, such as composition, crystallinity, and relative abundance.

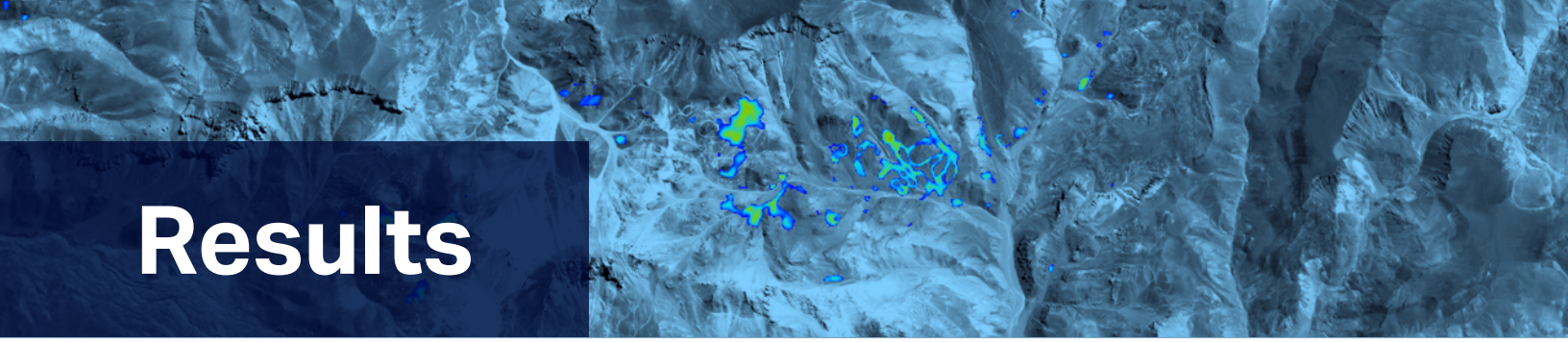

# Results

The following section displays the alteration images generated for each detected mineral, along with the supporting context images produced for this case study.

## List of Alteration Minerals

- 75m Silica Distribution
- 25m Opal/Chalcedony Distribution
- 25m Alunite Relative Abundance
- 25m K-Alunite Distribution
- 25m Na-Alunite Distribution
- 25m Kaolinite Distribution
- 25m Dickite Distribution
- 25m Pyrophyllite Distribution
- 25m Muscovite Relative Abundance
- 25m High-Aluminum Muscovite Distribution
- 25m Low-Aluminum Muscovite Distribution
- 25m Illite Distribution
- 25m Montmorillonite Distribution
- 25m Chlorite/Epidote Relative Abundance
- 25m Calcite Distribution
- 25m Hematite Distribution
- 25m Goethite Distribution
- 25m Jarosite Distribution

## List of Context Images

The context images are meant to be used in conjunction with the alteration mineral files to provide additional spatial context to the results.

- 10m Colour Image
- 10m Geology Enhanced Image
- 10m Greyscale Image
- 25m Vegetation Intensity Image
- 25m SWIR Enhanced Image
- 10m Sabins Composite Image
- 10m Sultan Composite Image

# Alteration Images

**Figure 5.** Map of silica distribution. Silica or quartz is a common mineral in most rock types. Silica flooding is common in many types of hydrothermal ore systems, especially within the lithocap environment, and may help indicate broad zones of hydrothermal alteration.

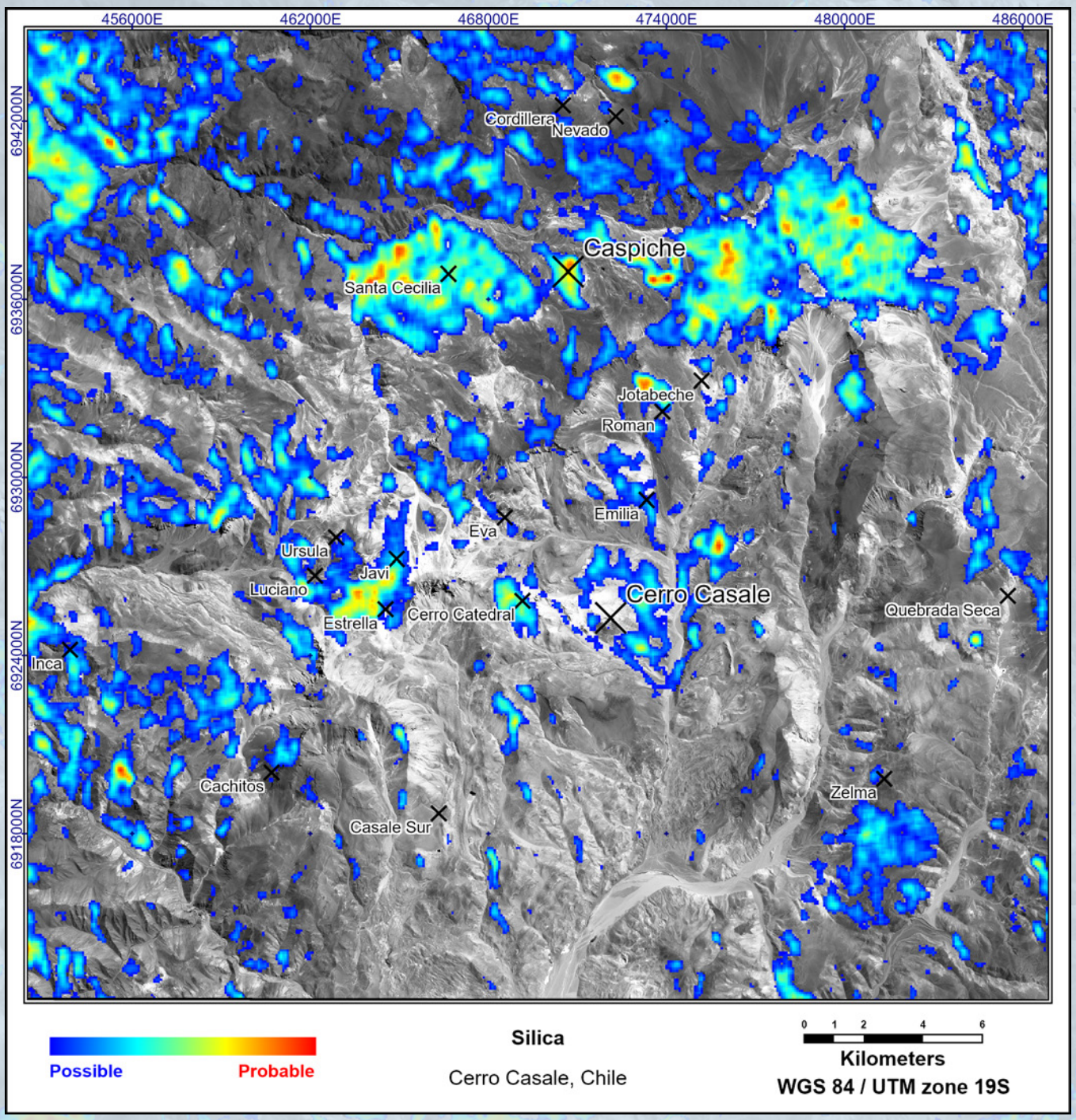

**Figure 6.** Map of opal/chalcedony distribution. Opal and chalcedony are types of silica that can be identified using SWIR data because they contain structural water. In porphyry-epithermal systems, opal/chalcedony can sometimes indicate paleo-water tables, fluid outflow zones, silica sinters, and, at times, can be found associated with the vuggy silica zones at the core of high-sulfidation epithermal systems.

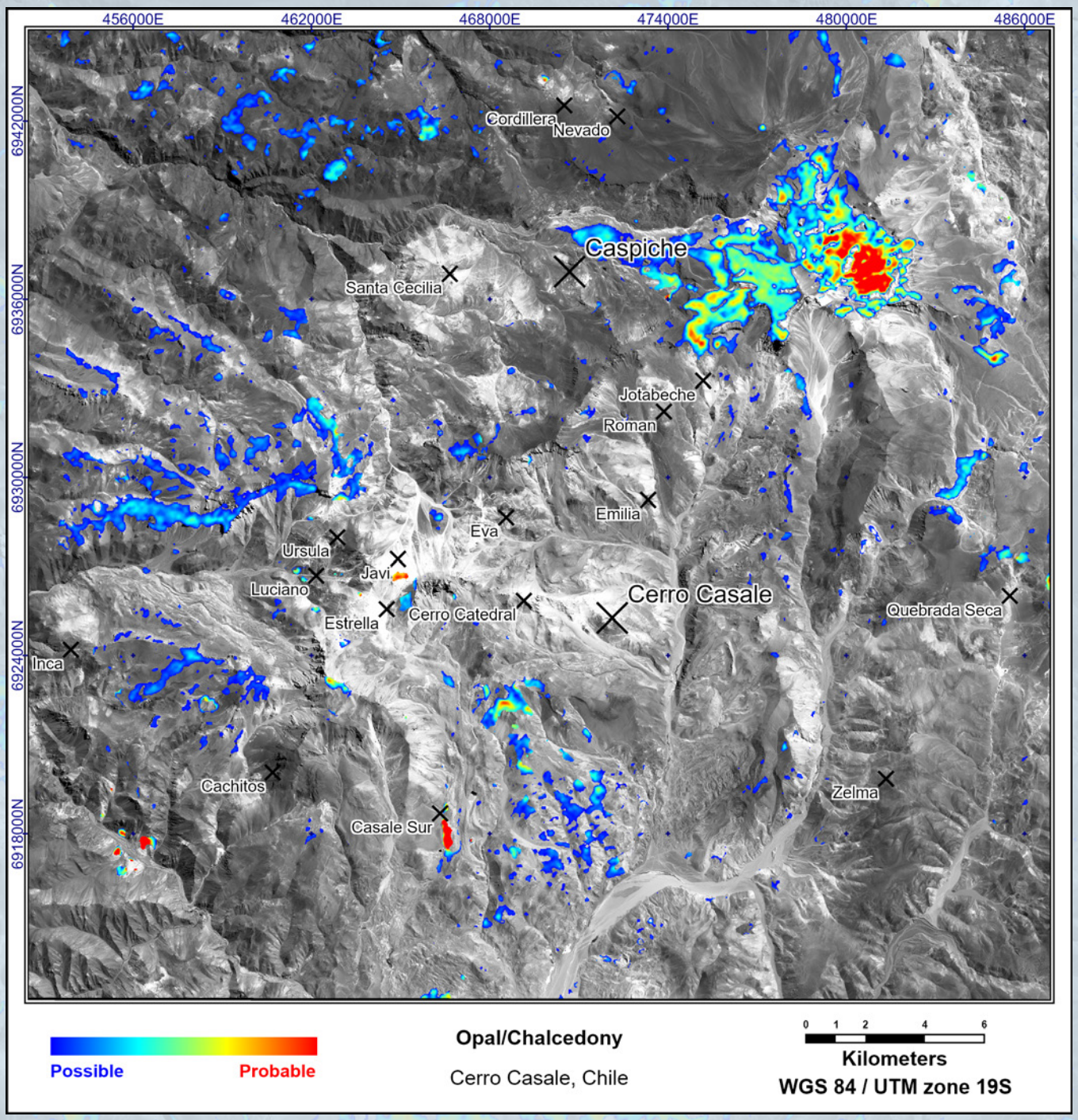

**Figure 7.** Map of alunite relative abundance. Alunite is a key alteration mineral in highly acidic advanced argillic alteration zones. It often forms near the center of high-sulfidation epithermal systems just outside of the main ore zones within the lithocap. Advanced argillic alteration can sometimes overprint or telescope porphyry systems, as seen at Cerro Casale and Caspiche.

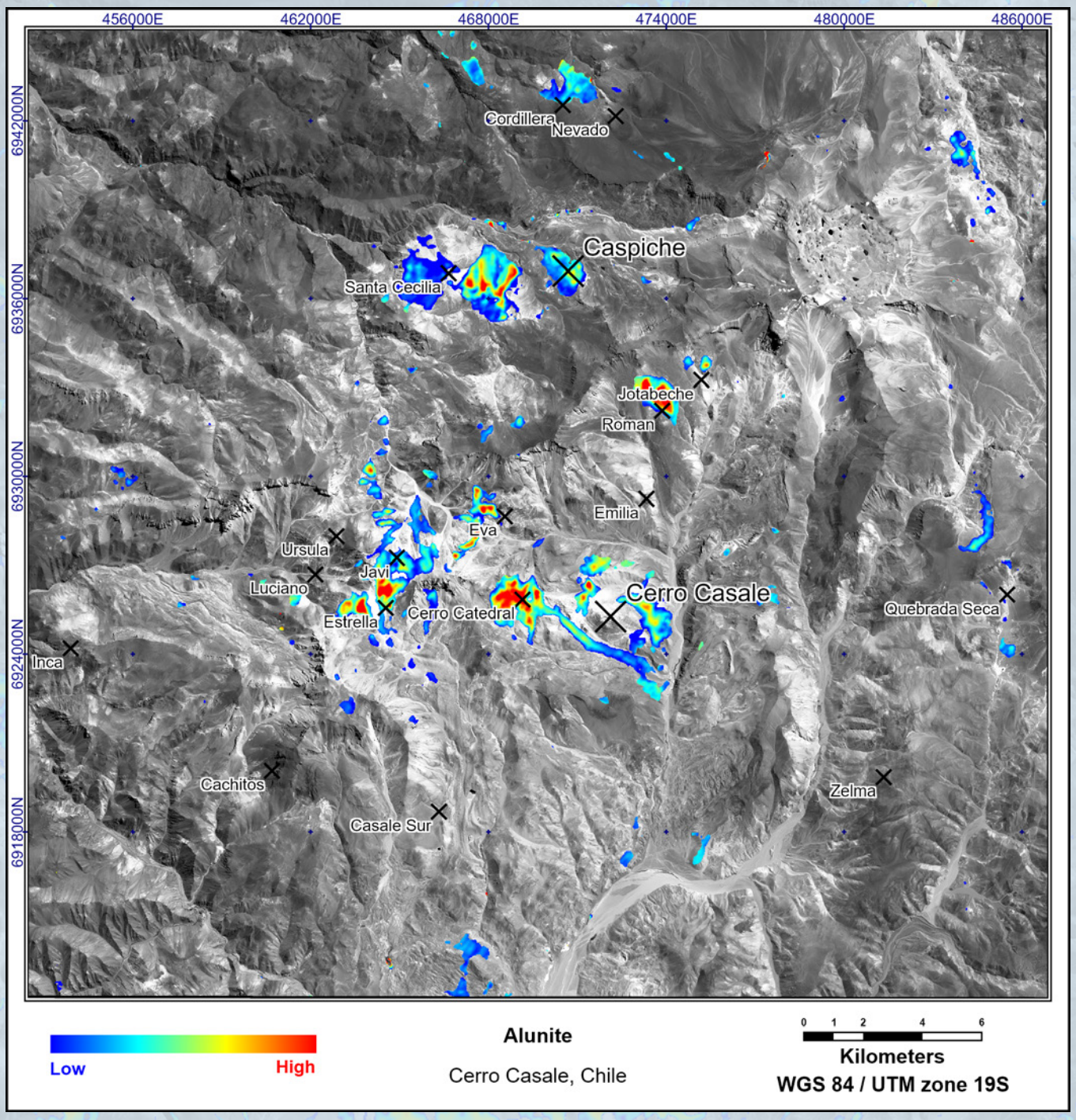

**Figure 8**. Map of Na-alunite distribution. Alunite forms a solid solution with compositional endmembers that are sodium (Na)-rich and potassium (K)-rich. Mapping sodium-rich alunite can sometimes be an indicator of higher-temperature alteration related to hypogene processes.

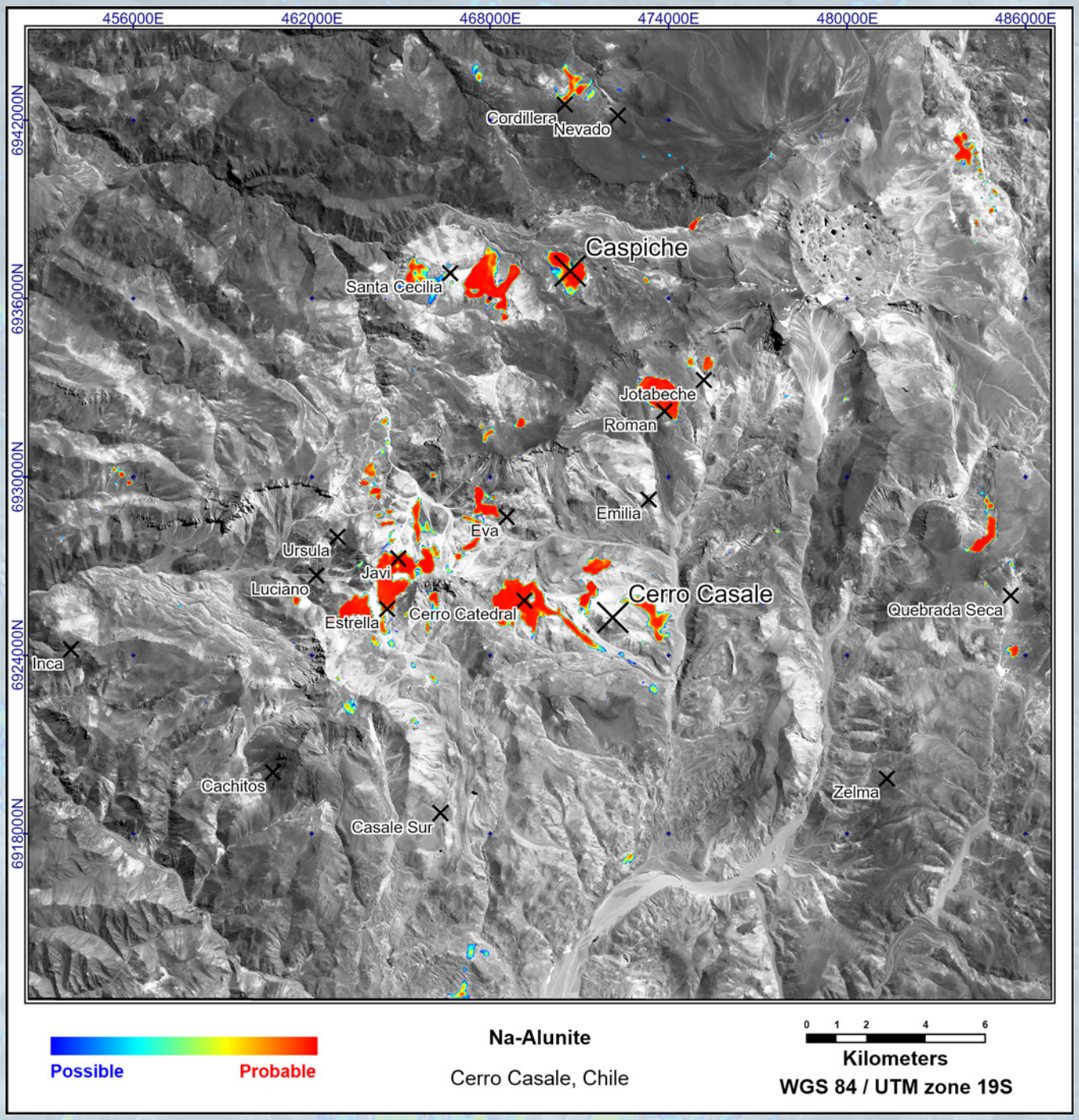

**Figure 9.** Map of K-alunite distribution. Alunite forms a solid solution with compositional endmembers that are sodium (Na)-rich and potassium (K)-rich. Mapping potassium-rich alunite can help differentiate alunite formed through supergene processes rather than hypogene processes.

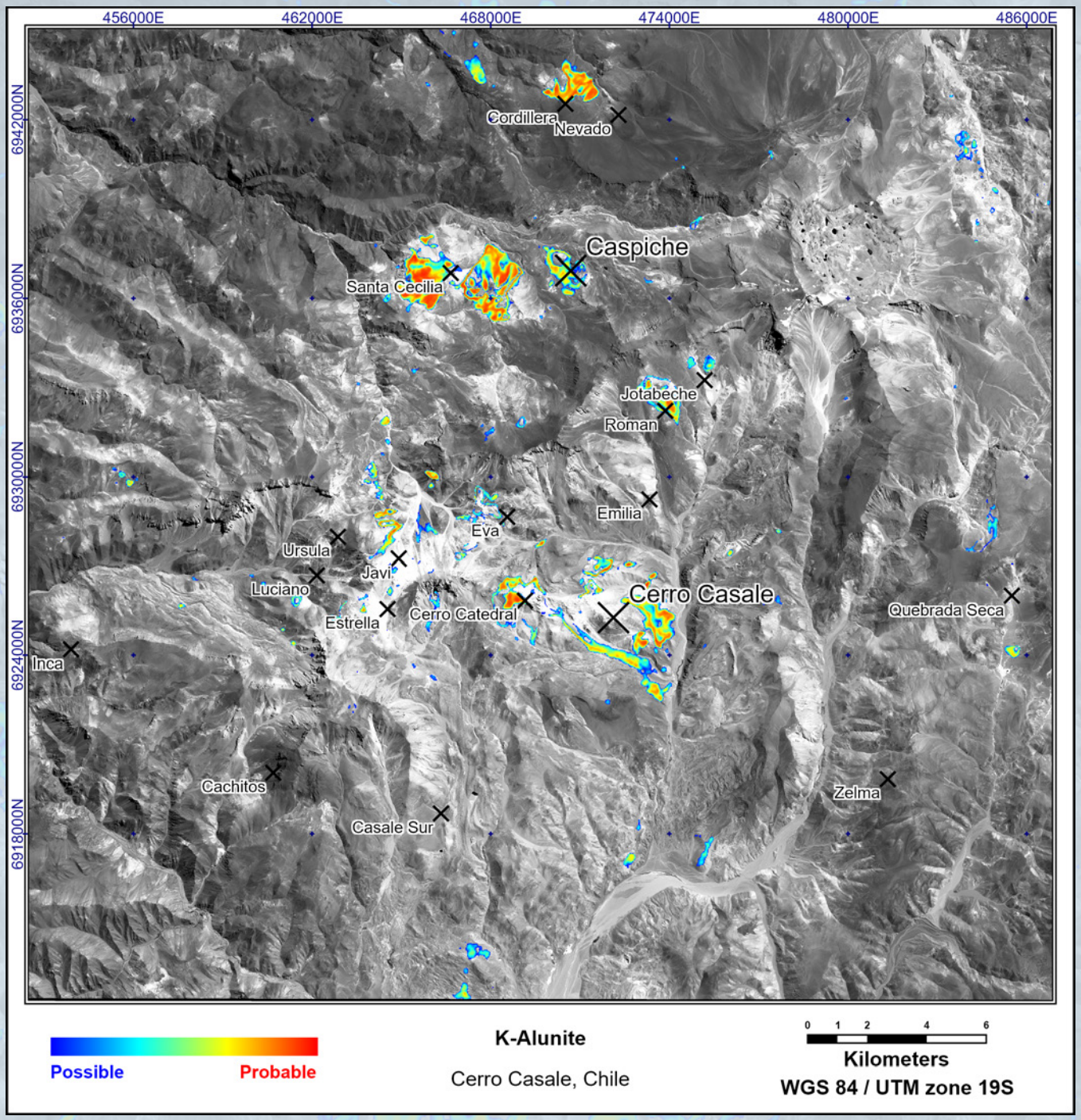

**Figure 10**. Map of kaolinite distribution. Kaolinite is an important argillic alteration mineral and can often be a good indicator to hydrothermal ore forming systems occurring within the argillic and advanced argillic zones of porphyry-epithermal systems. Kaolinite forms through many other processes so its presence has to be considered in context with other common hydrothermal indicator minerals. This result likely includes both poorly crystalline kaolinite and well crystalline kaolinite.

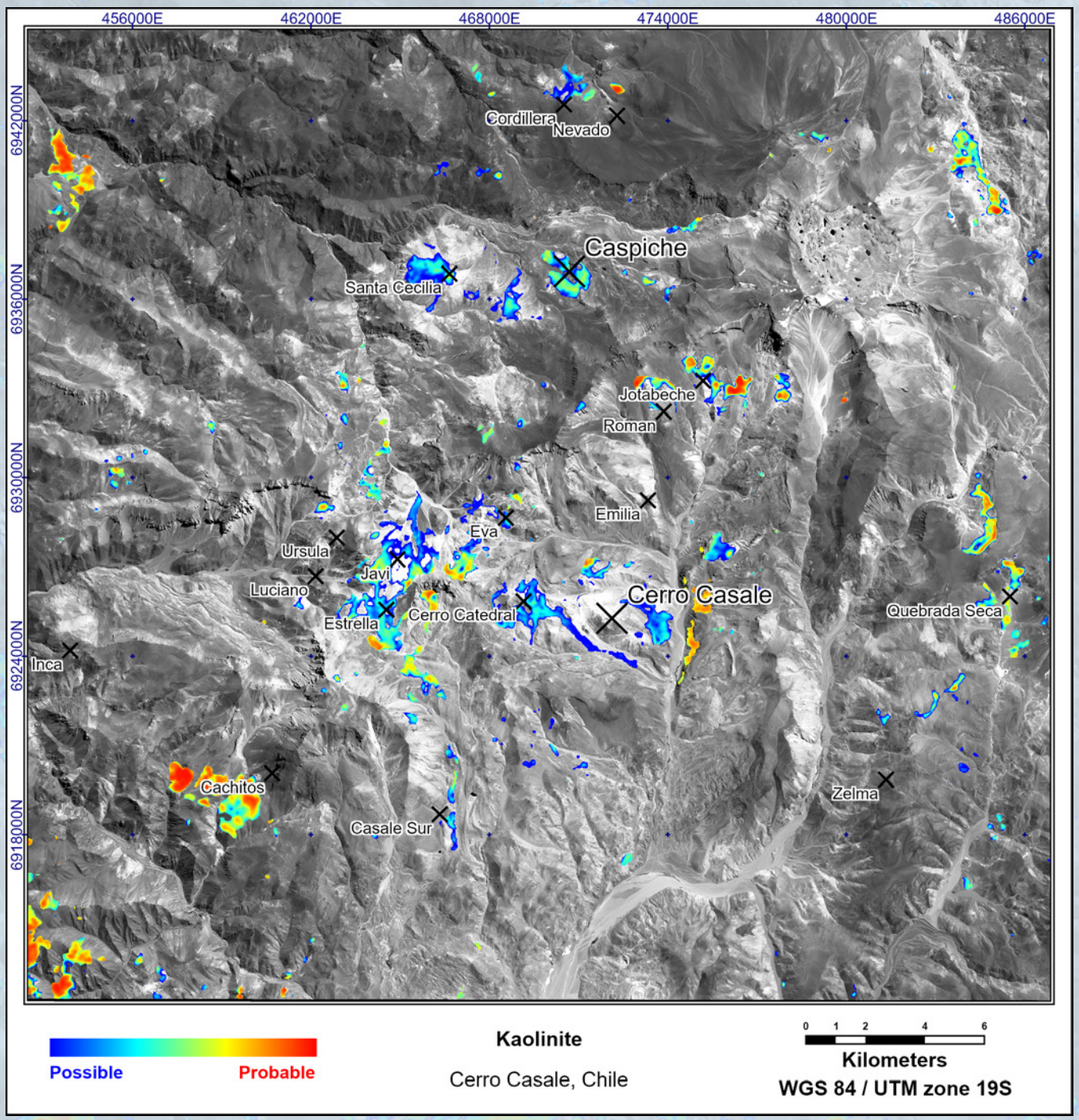

**Figure 11.** Map of dickite distribution. Dickite is a kaolinite-group mineral which often occurs in highly acidic advanced argillic alteration zones in the lithocap. Dickite typically forms close to the fluid upflow zones which then transitions outwards into kaolinite. This result likely also includes some areas containing well-crystalline kaolinite as they can be very spectrally similar.

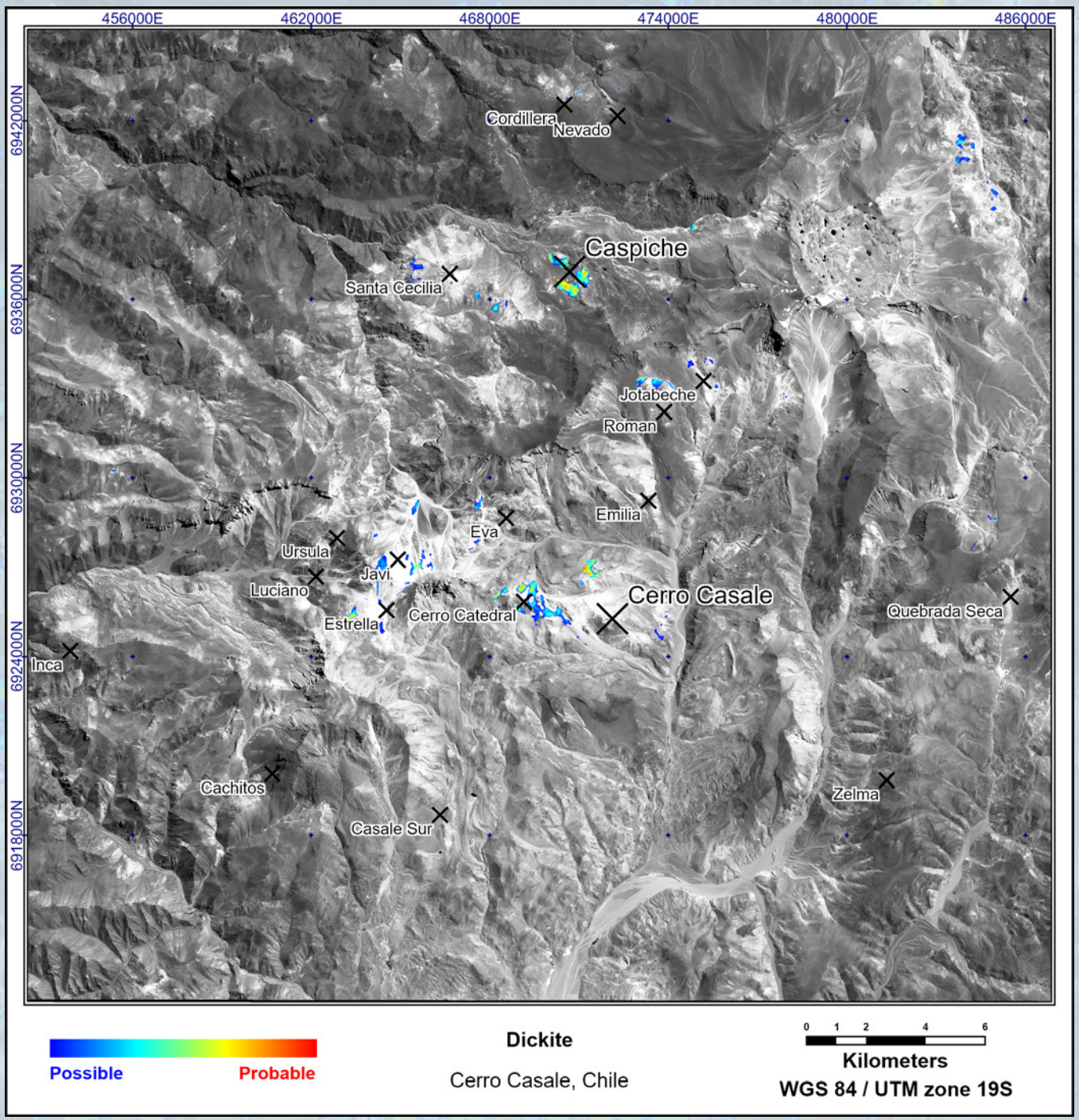

**Figure 12**. Map of pyrophyllite distribution. Pyrophyllite is a key indicator mineral of high-temperature advanced argillic conditions occurring near the base of the high-sulfidation lithocap near the core of the system, marking the upper transition to the deeper porphyry environment.

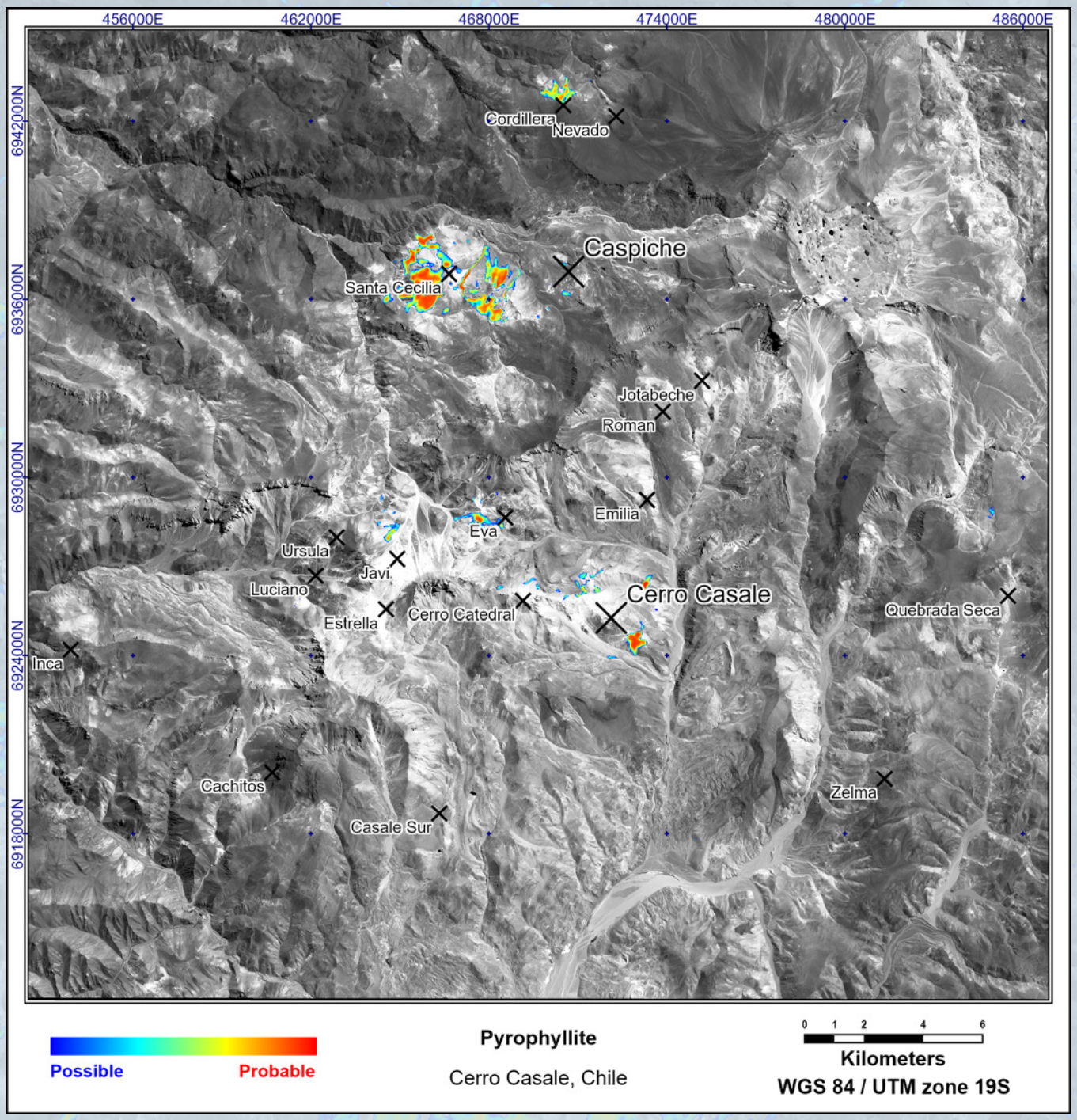

**Figure 13.** Map of jarosite distribution. Jarosite forms within highly acidic oxidizing sulfate-rich conditions common in both hypogene and supergene conditions. In hypogene environments, it typically occurs as part of the advanced argillic assemblage of high-sulfidation systems within the lithocap. In supergene conditions, it commonly occurs in gossans formed due to the weathering of sulfide minerals often associated with ore bodies.

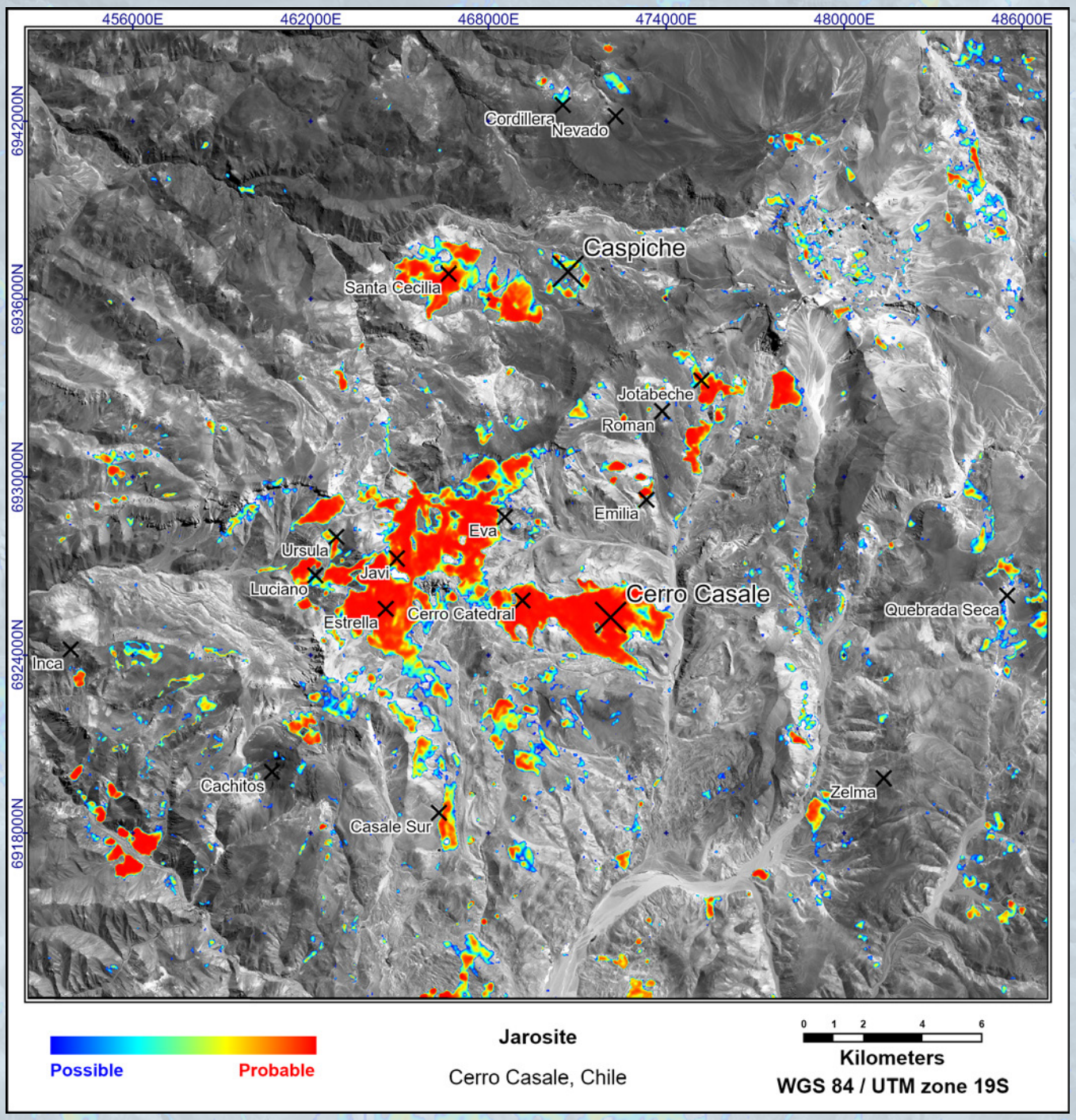

**Figure 14**. Map of muscovite relative abundance. Type of white mica. Fine-grained muscovite (sericite) tends to form in the phyllic alteration zones of porphyry systems. Its abundance can be a good indicator of the intensity of the phyllic alteration zone. It is also a common mineral in metamorphic and granitic rocks, so its presence should be used in conjunction with other common hydrothermal alteration minerals. Differentiating muscovite from illite helps better distinguish between hydrothermal/metamorphic and supergene processes.

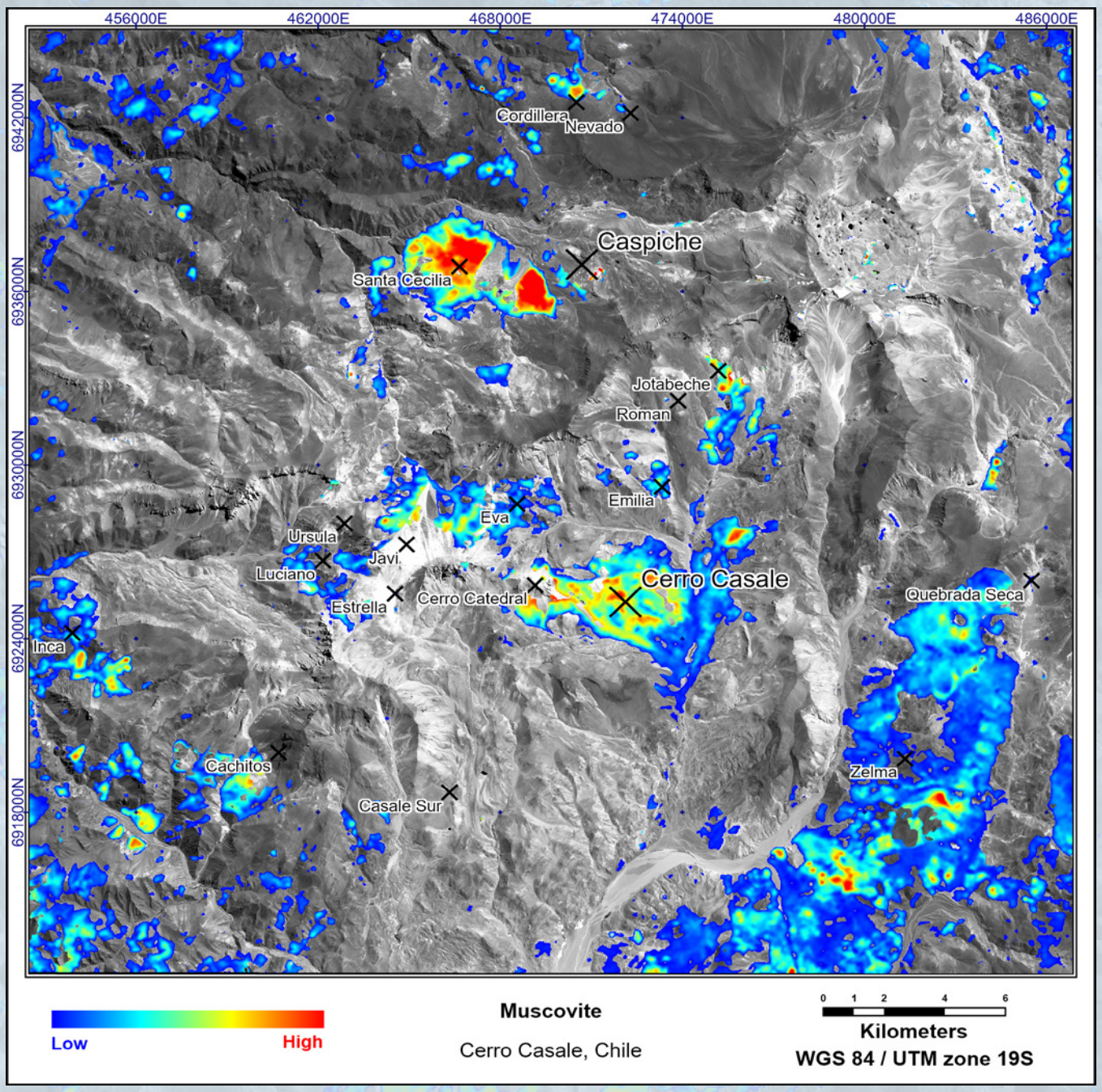

**Figure 15.** Map of high-Al muscovite distribution. Type of white mica. High-aluminum (Al) muscovite can be differentiated based on a downshifted wavelength of the main diagnostic feature. A higher aluminum content of the muscovite can indicate higher temperature processes, meaning it can sometimes be used as a vector to the core of the porphyry system. This can sometimes vary due to the interaction of the hydrothermal fluids with various compositions of wallrock.

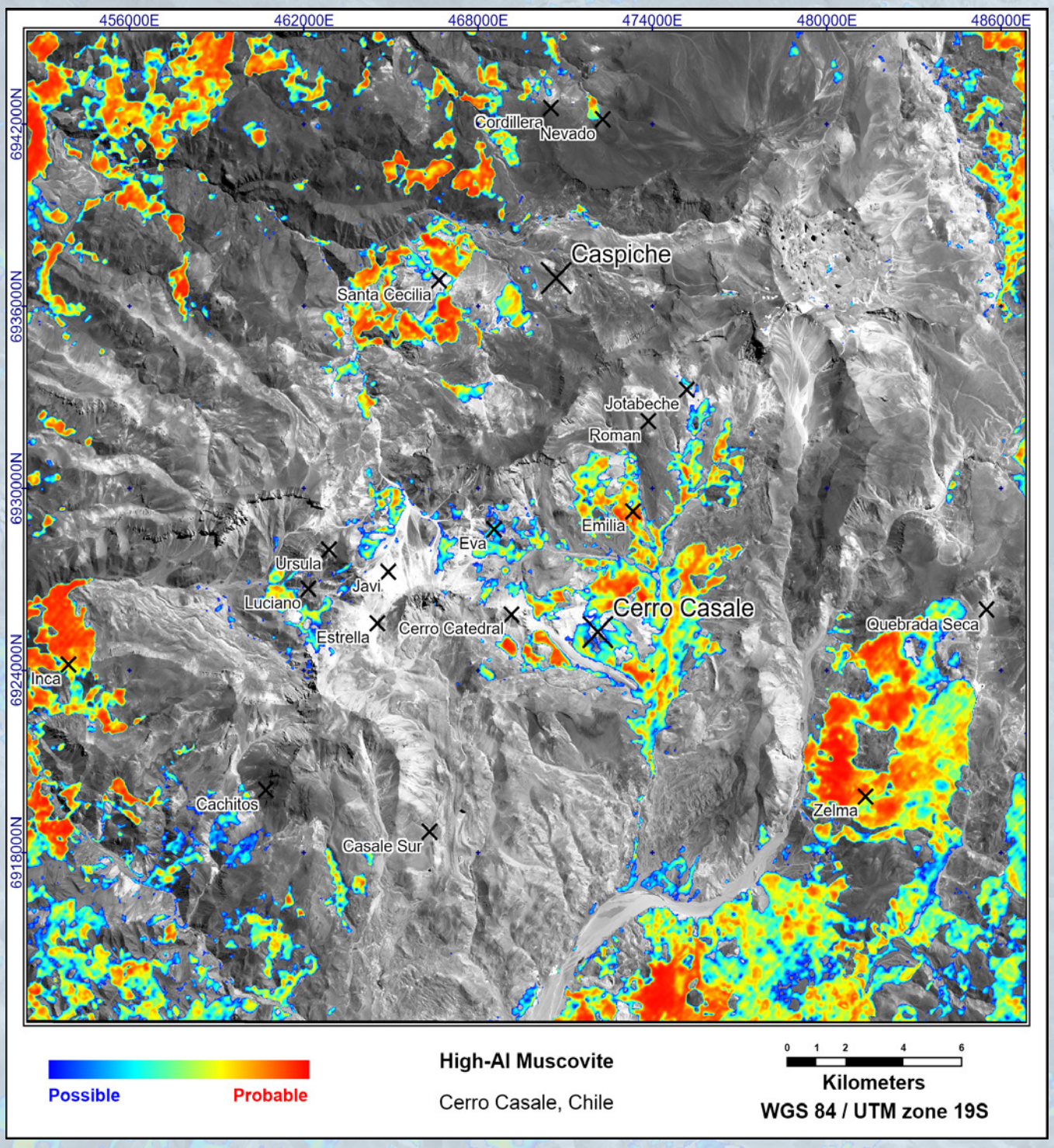

**Figure 16**. Map of low-Al muscovite distribution. Type of white mica. Low-aluminum (Al) muscovite can be differentiated based on an upshifted wavelength of the main diagnostic feature. A lower aluminum content of the muscovite can indicate more iron and silica-rich compositions, which typically occur more distal from the porphyry center. In some cases, this can be inversed due to the hydrothermal fluids interacting with iron-rich wall rocks.

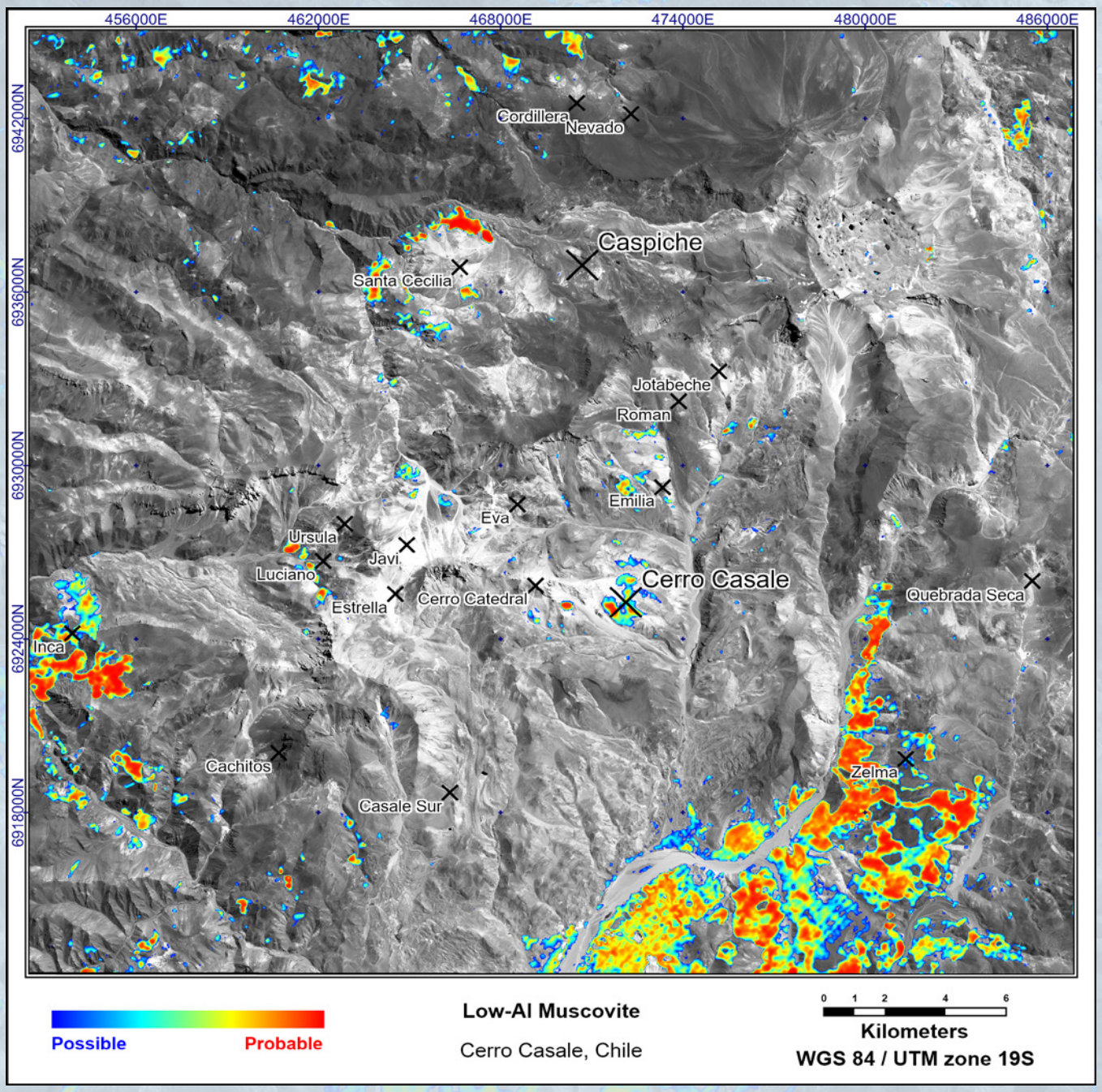

**Figure 17.** Map of illite distribution. Illite is a clay mineral that often appears similar to muscovite both spectrally and in hand sample; however, it tends to occur in lower-temperature argillic alteration environments, such as in shallow hydrothermal systems, including low-sulfidation epithermal systems, or from burial metamorphism/ near-surface weathering of feldspar minerals.

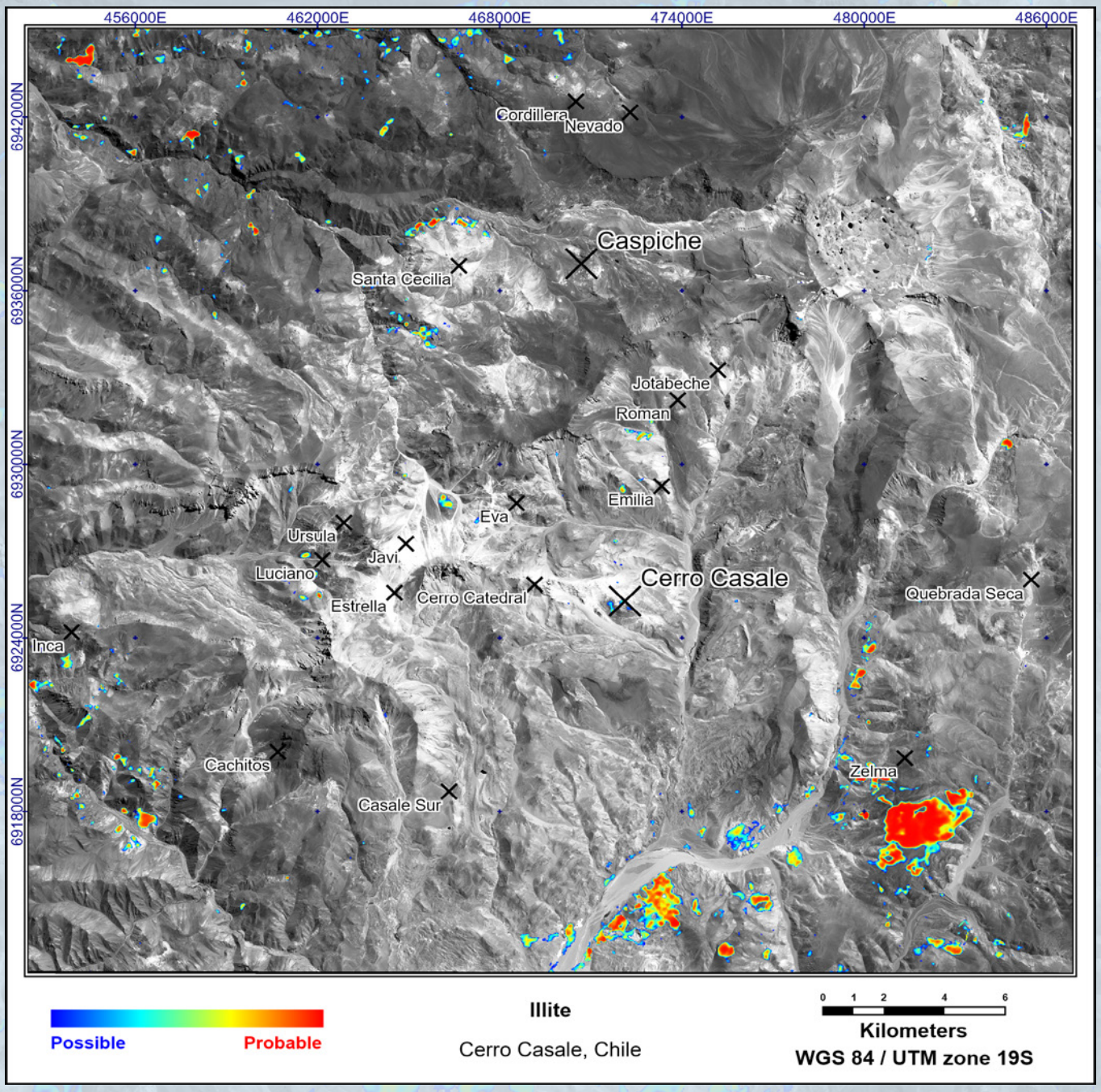

**Figure 18**. Map of montmorillonite distribution. Montmorillonite is a smectite clay mineral that can sometimes resemble sericite or illite in a hand sample. Montmorillonite typically indicates a much cooler, distal environment in hydrothermal systems, often forming near the edges of the argillic alteration zones. Montmorillonite is a common mineral in soils, sedimentary rocks, and weathering profiles; therefore, its occurrence should be considered in conjunction with other hydrothermal minerals.

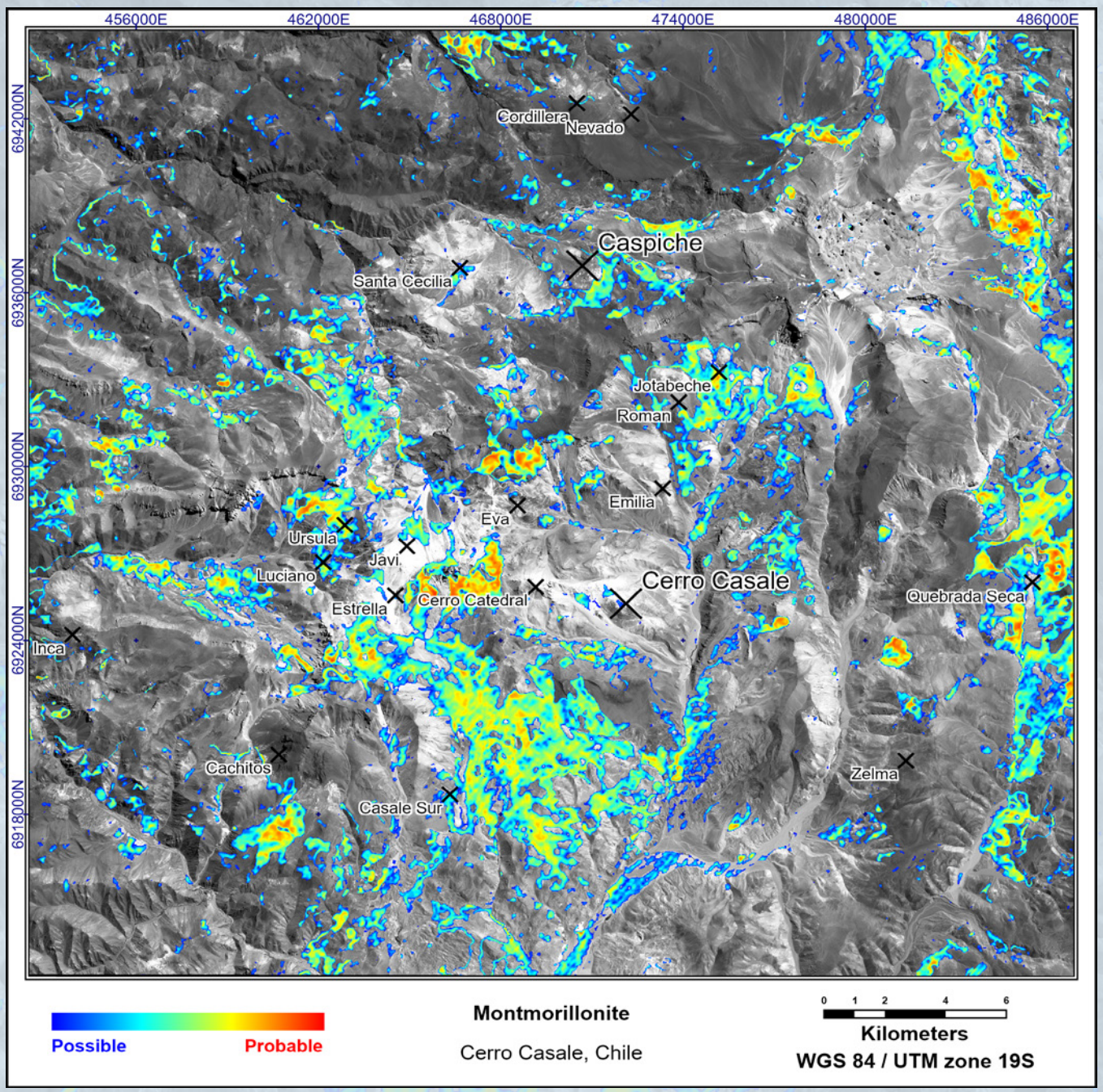

**Figure 19.** Map of chlorite/epidote relative abundance. Chlorite and epidote can indicate propylitic alteration zones, which occur in the cooler, neutral pH peripheral zones of porphyry-epithermal systems. Propylitic alteration is often the most extensive alteration zone and can help indicate ore bodies even when more proximal alteration zones are obscured. It is also a common mineral in some primary rock types, so it may not always be related to hydrothermal events. Chlorite/epidote chemistry, such as Fe vs. Mg content, can sometimes be used as a vector to the high-temperature core. This is possible with hyperspectral data, but is not shown here due to the minimal response of chlorite/epidote.

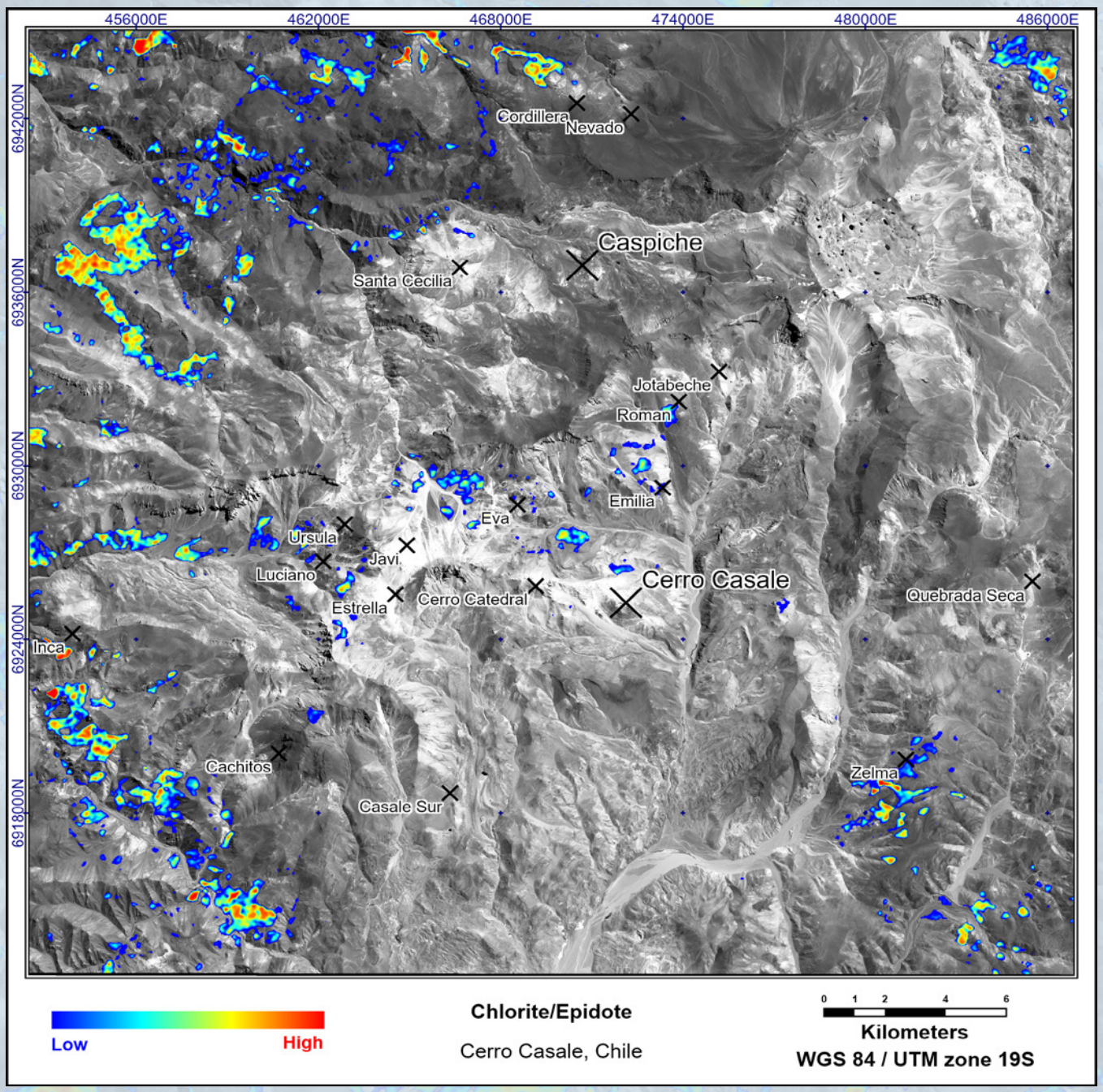

**Figure 20**. Map of calcite distribution. Calcite is a common hydrothermal alteration mineral in porphyry-epithermal systems, most often occurring alongside chlorite/epidote in the propylitic alteration zone. It also sometimes forms as a late-stage fracture that fills in porphyry-epithermal systems. It commonly occurs as primary calcite in carbonate-rich rocks such as limestones.

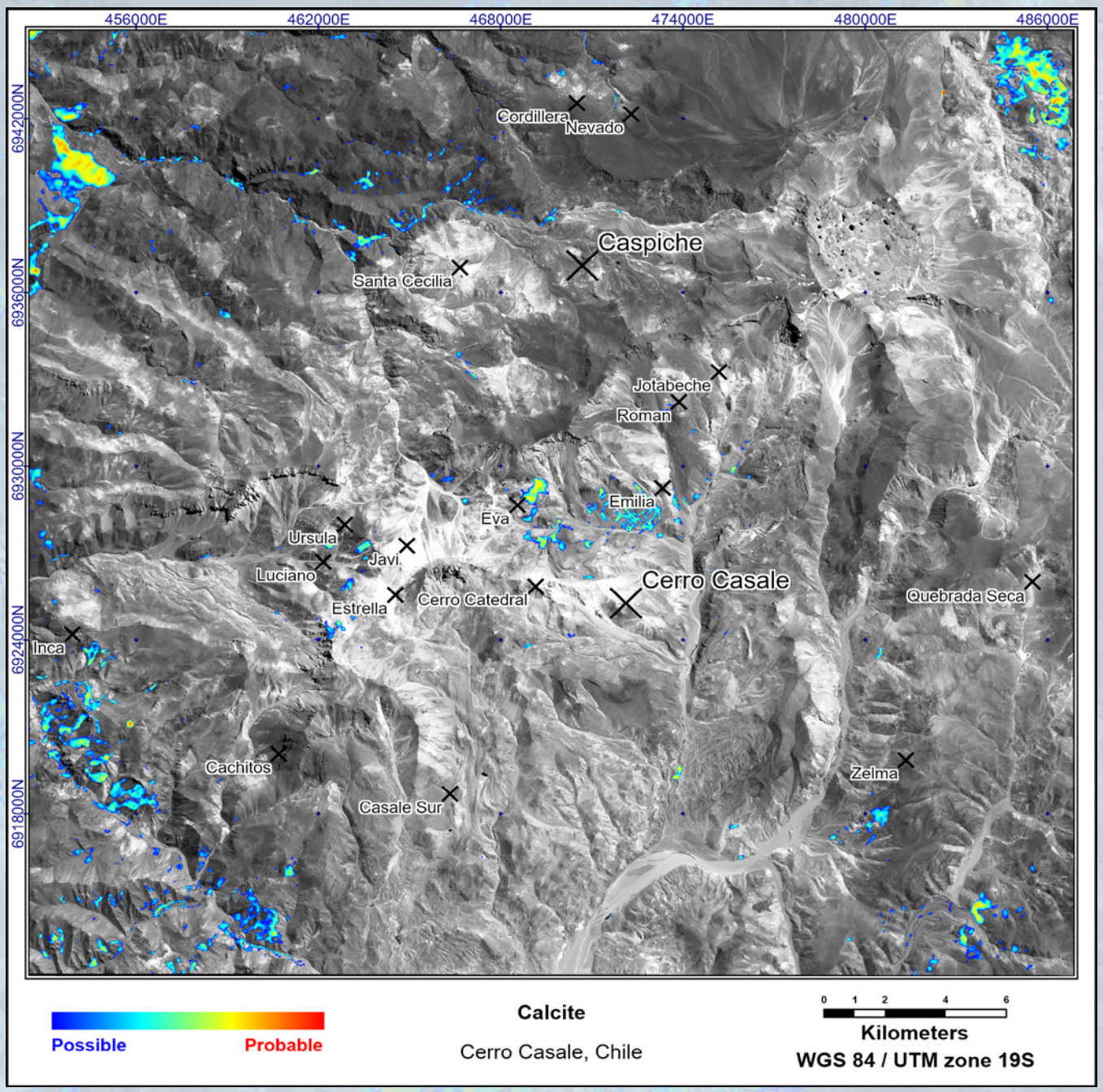

**Figure 21.** Map of goethite distribution. Goethite is a hydrous iron-oxide mineral that forms due to the near-surface weathering of primary iron-bearing minerals. Similarly to jarosite, it forms in supergene conditions commonly occurring in gossans formed due to the weathering of sulfide minerals associated with ore bodies. However, jarosite is often more indicative of very acidic sulfate weathering conditions common in advanced argillic zones of high-sulfidation epithermal deposits.

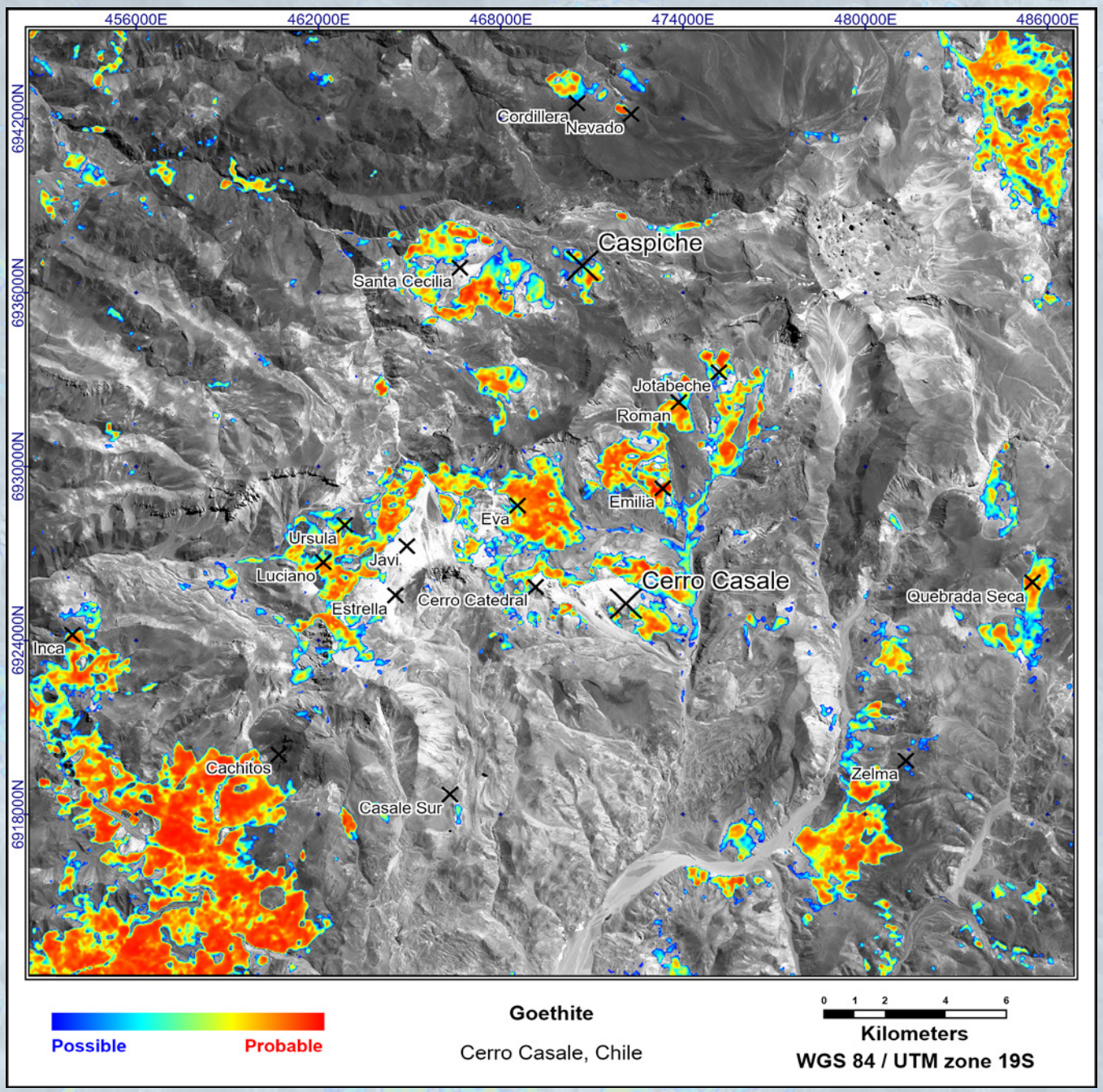

**Figure 22**. Map of hematite distribution. Hematite is a common iron oxide mineral in some primary lithologies and sometimes occurs in hydrothermal deposits. In porphyry-epithermal systems, hematite typically indicates highly oxidizing conditions. It most commonly occurs with advanced argillic alteration minerals, but may also develop at depth where oxidized hypogene fluids overprint earlier magnetite. It is also found in the supergene environment, resulting from the prolonged weathering and dehydration of goethite in gossans.

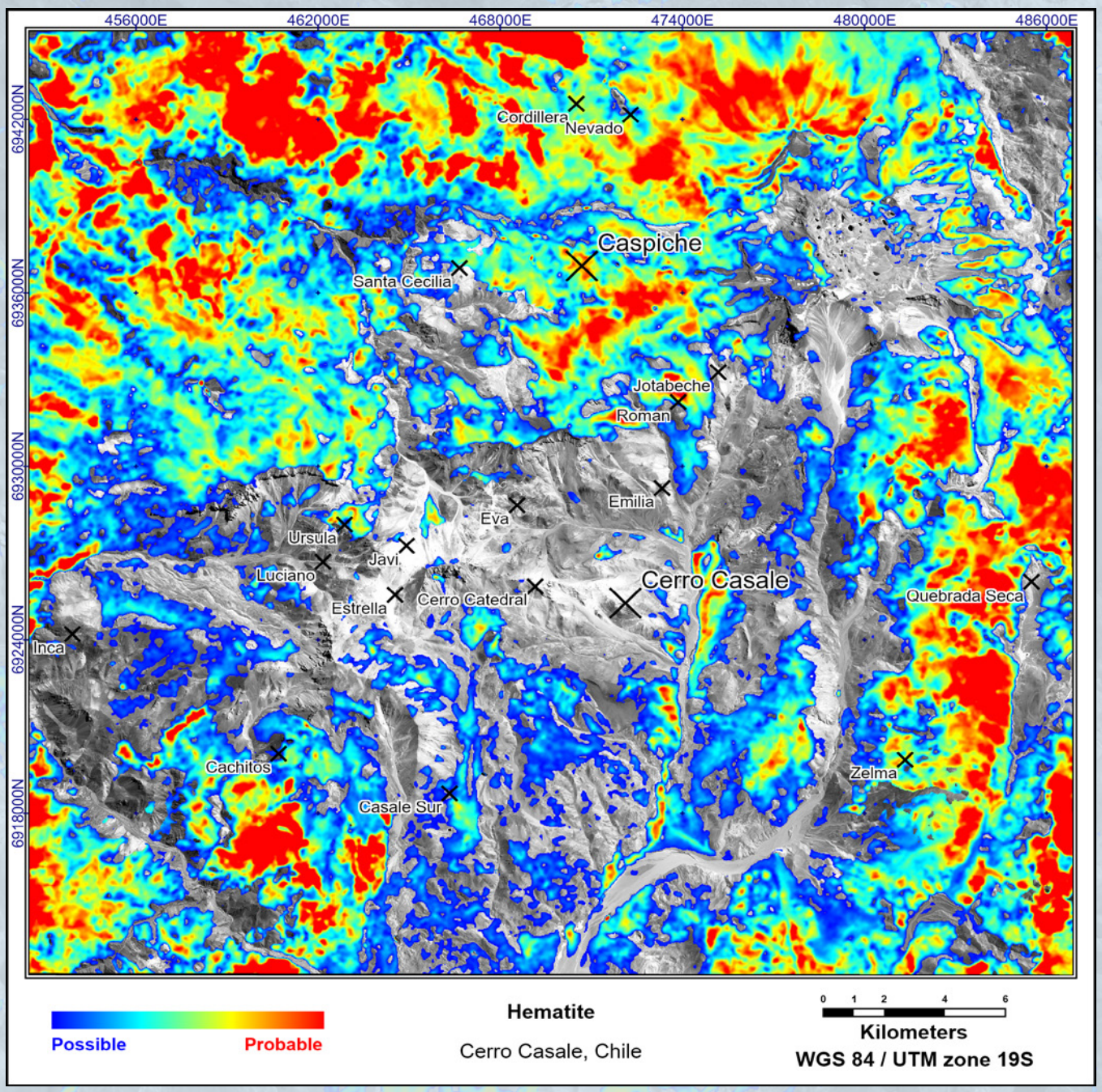

# Context Images

**Figure 23.** Colour Image. RGB image showing the project area in natural colour.

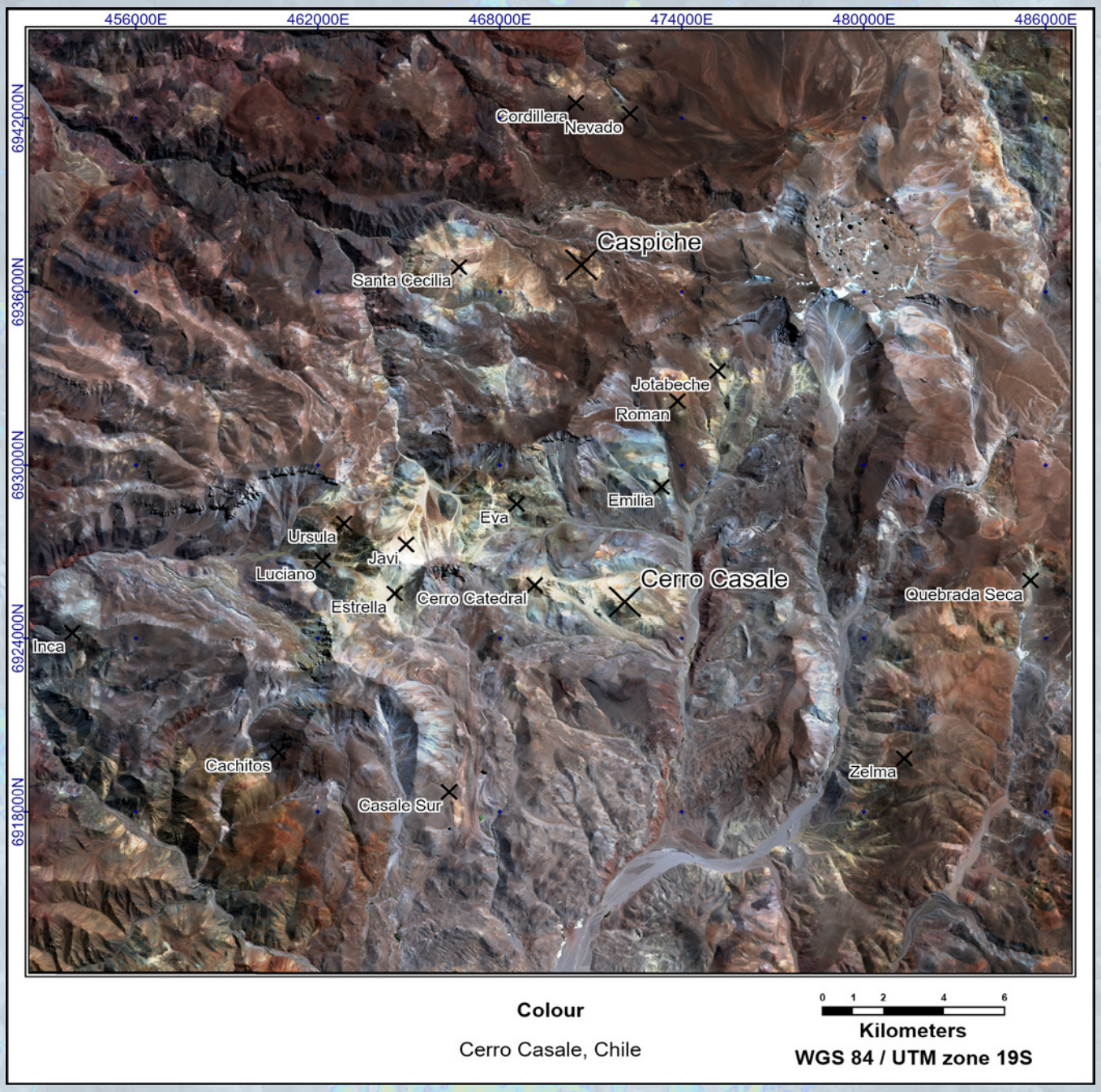

**Figure 24**. Greyscale Image. Primarily used as a base image when overlaying the mineral GeoTIFFs or shapefiles.

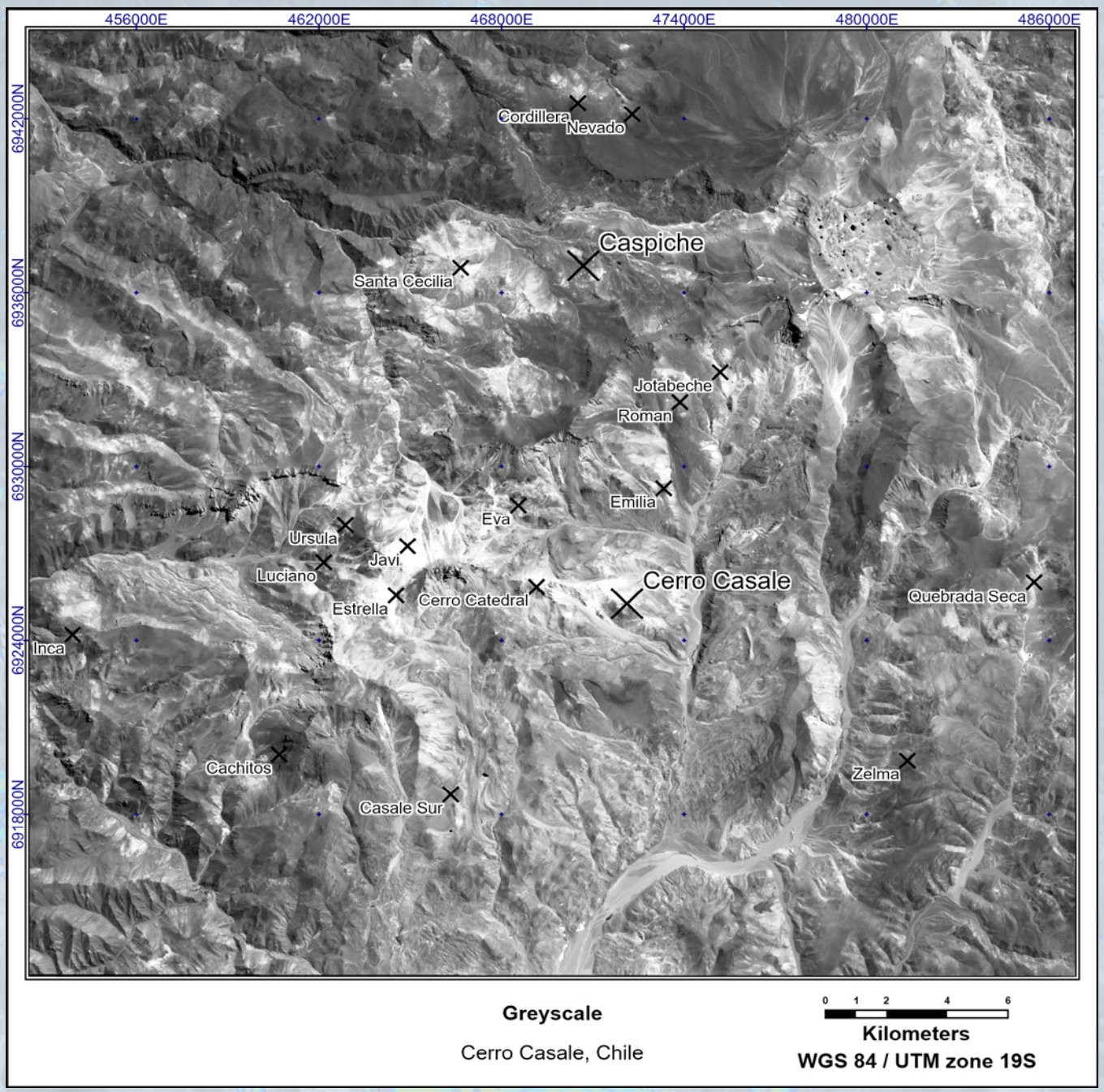

**Figure 25.** Geology Enhanced Colour Image. RGB image combining VNIR and SWIR bands to better highlight changes in the lithologies and alteration not visible in the colour image.

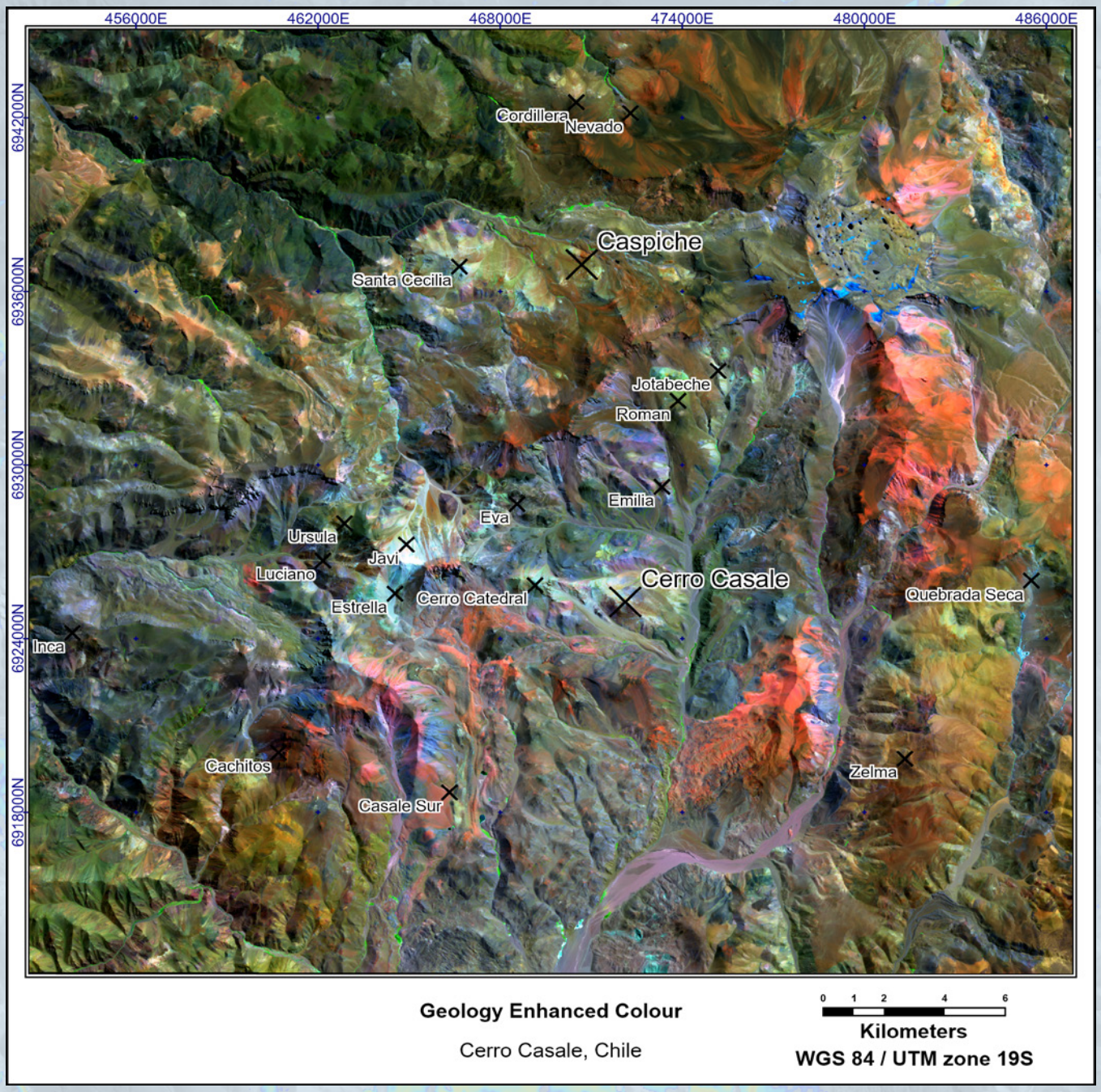

**Figure 26**. SWIR Enhanced Composite Image. RGB composite image, which combines various SWIR responsive minerals to display them as different colours. Alunite often appears blue, kaolinite purple, white mica pink, chlorite red, and opal/chalcedony orange.

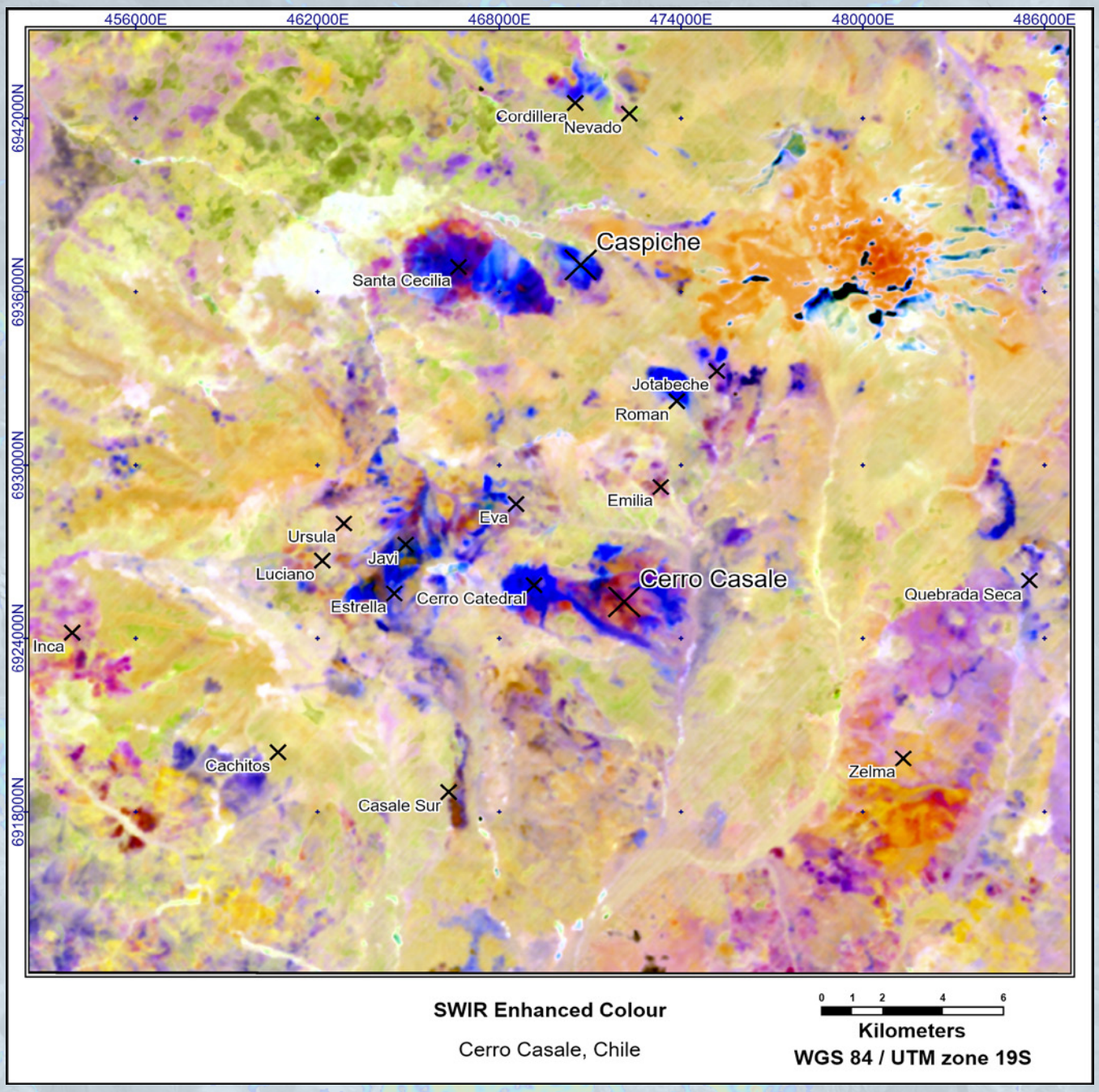

**Figure 27.** Sabins Composite Image. RGB composite image, which uses a combination of spectral indices to better highlight the variation in primary lithologies and alteration minerals.

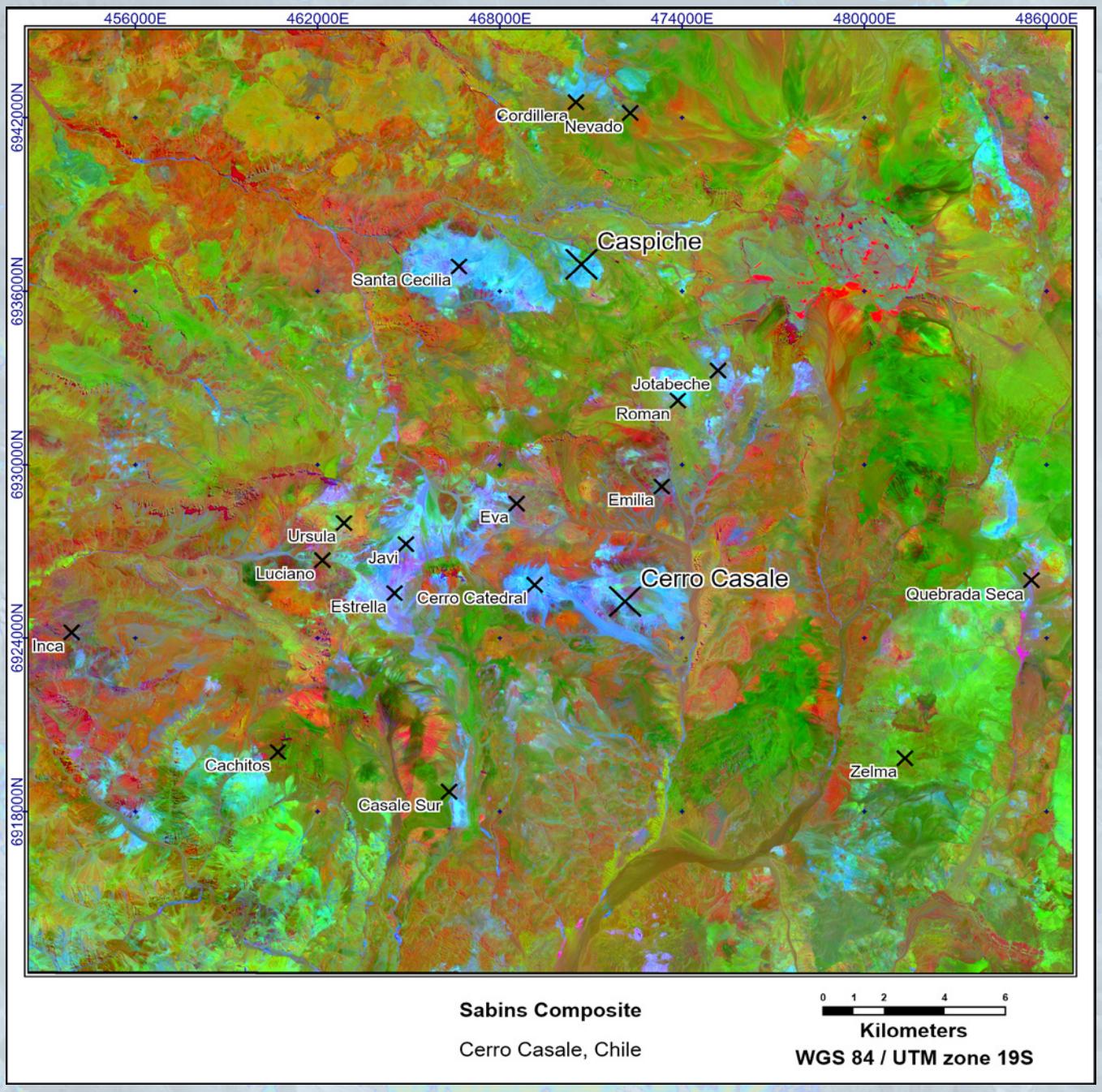

**Figure 28**. Sultan Composite Image. RGB composite image, which uses a combination of spectral indices to better highlight the variation in primary lithologies and alteration minerals.

**Figure 29.** Vegetation intensity image. RGB image that shows the distribution of vegetation in the project area. Alteration minerals cannot be mapped when the vegetation is too intense.

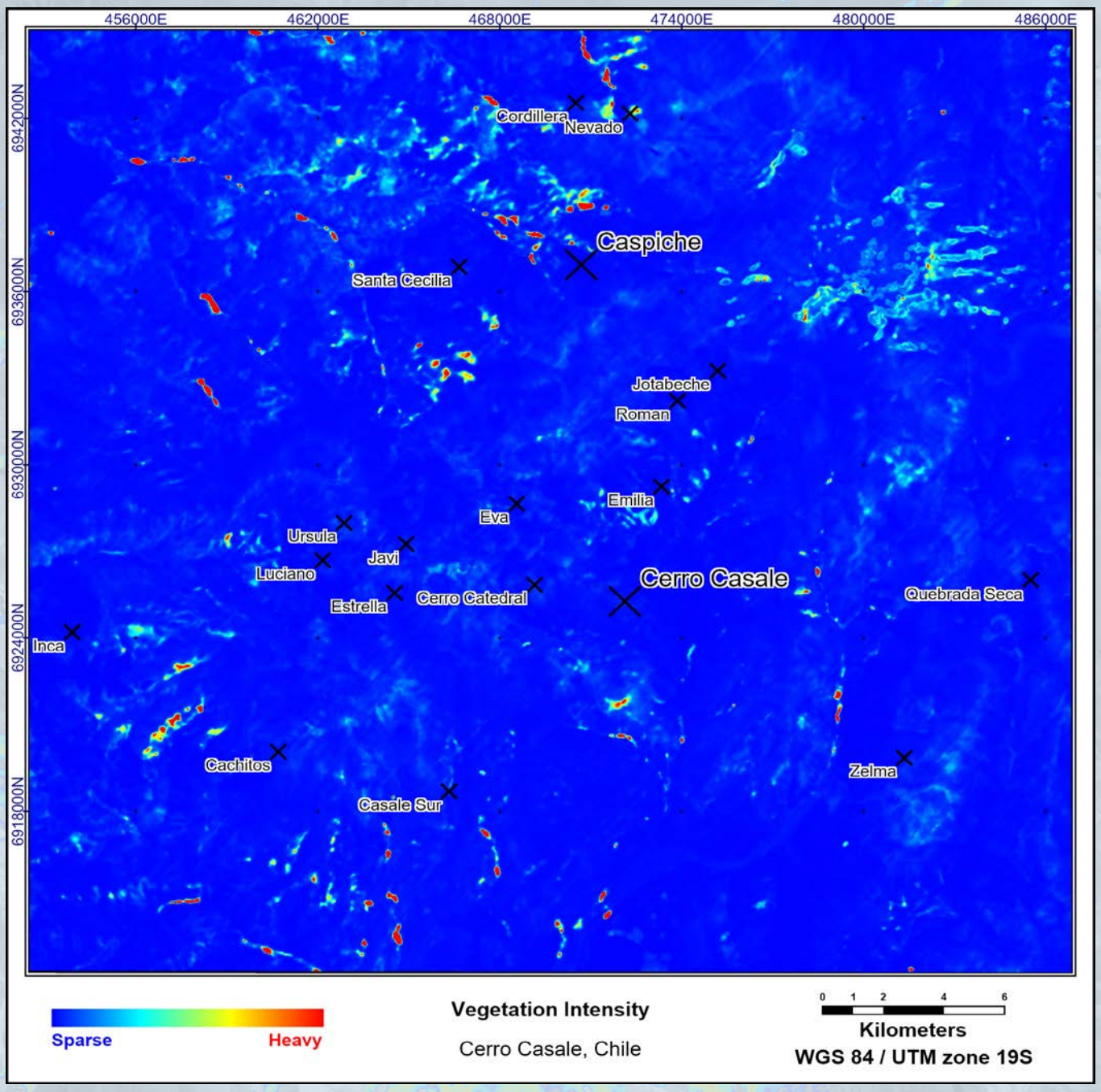

## Sources


Sillitoe, R. H., Tolman, J., & Kerkvoort, G. V. (19912013). Geology of the Caspiche Porphyry Gold-Copper Deposit, Maricunga Belt, Northern Chile. Economic Geology and the Bulletin of the Society of Economic Geologists. https://doi.org/10.2113/econgeo.108.4.585

Palacios, Carlos & Herail, G. & Townley, Brian & Maksaev, Victor & Sepúlveda, Fabián & de Parseval, Philippe & RIVAS, PABLO & LAHSEN, ALFREDO & Parada, Miguel A. (2001). The composition of gold in the Cerro Casale gold-rich porphyry deposit, Maricunga belt, Northern Chile. Canadian Mineralogist - CAN MINERALOG. 39. 907-915. 10.2113/gscanmin.39.3.907.

Henderson, R., & Eng, P. (2010). *Cerro Casale Project Northern Chile NI 43-101 Technical Report Prepared for: Kinross Gold Corporation.* https://minedocs.com/12/Cerro%20Casale_02182010_FS.pdf

Major Mines & Projects | Norte Abierto (Cerro Casale) Project. https://miningdataonline.com/property/3063/Norte-Abierto-Cerro-Casale-Project.aspx


REQUEST A **QUOTE**

PHOTOSAT

---

**PhotoSat is a trusted partner supporting safe and responsible mining projects worldwide. With over 200 years of combined engineering, geology, and geophysics expertise, PhotoSat offers innovative solutions that span exploration to closure. PhotoSat is the leading expert in satellite solutions produced using proprietary software and deep-learning models designed and tested for optical satellite data.**

**Better Data. Better Decisions.**

---


**PhotoSat Information Ltd.**
**#580—1188 West Georgia Street**
**Vancouver BC Canada V6A4E2**
**1-604-681-9770**

**PhotoSat.ca**